

Accepted Manuscript

Synthesis of novel *S*-linked dihydroartemisinin derivatives and evaluation of their anticancer activity

Rajesh Gour, Faiz Ahmad, Santosh Kumar Prajapati, Santosh Kumar Giri, Shibendra Kumar Lal Karna, K.P. Ravindranathan Kartha, Yuba Raj Pokharel



PII: S0223-5234(19)30537-9

DOI: <https://doi.org/10.1016/j.ejmech.2019.06.018>

Reference: EJMECH 11421

To appear in: *European Journal of Medicinal Chemistry*

Received Date: 12 March 2019

Revised Date: 24 May 2019

Accepted Date: 5 June 2019

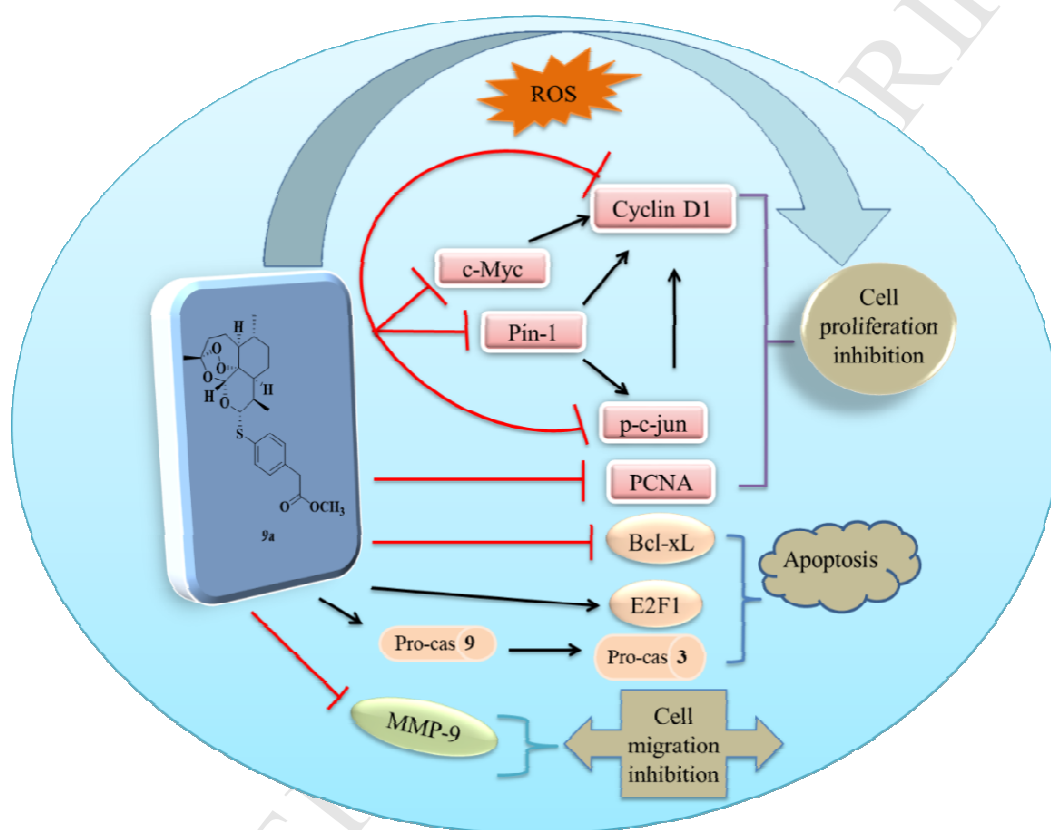
Please cite this article as: R. Gour, F. Ahmad, S.K. Prajapati, S.K. Giri, S.K. Lal Karna, K.P.R. Kartha, Y.R. Pokharel, Synthesis of novel *S*-linked dihydroartemisinin derivatives and evaluation of their anticancer activity, *European Journal of Medicinal Chemistry* (2019), doi: <https://doi.org/10.1016/j.ejmech.2019.06.018>.

This is a PDF file of an unedited manuscript that has been accepted for publication. As a service to our customers we are providing this early version of the manuscript. The manuscript will undergo copyediting, typesetting, and review of the resulting proof before it is published in its final form. Please note that during the production process errors may be discovered which could affect the content, and all legal disclaimers that apply to the journal pertain.

Graphical Abstract

Synthesis of novel *S*-linked dihydroartemisinin derivatives and evaluation of their anticancer activity

Rajesh Gour,^a Faiz Ahmad,^b Santosh Kumar Prajapati,^a Santosh Kumar Giri,^a Shibendra Kumar Lal Karna,^b Yuba Raj Pokharel,^{b*} K. P. Ravindranathan Kartha^{a*}



Synthesis of novel S-linked dihydroartemisinin derivatives and evaluation of their anticancer activity

#Rajesh Gour,^a #Faiz Ahmad,^b Santosh Kumar Prajapati,^a Santosh Kumar Giri,^a Shibendra Kumar Lal Karna,^b K. P. Ravindranathan Kartha,^{a*} Yuba Raj Pokharel^{b*}

^aDepartment of Medicinal Chemistry, National Institute of Pharmaceutical Education and Research, S.A.S Nagar, Punjab-160062. India and

^bFaculty of Life Sciences and Biotechnology, South Asian University, New Delhi- 110021, India *E-mail: rkartha@niper.ac.in; yyp@sau.ac.in

Rajesh Gour^a & Faiz Ahmad^b equally contributed to this manuscript

Abstract

We report herein the synthesis and anticancer activity of a set of novel S-linked artemisinins bearing an aliphatic/aromatic/heterocyclic nucleus as a substituent on the sulfur. The compounds were prepared from artemisinin via its lactol-form by an acid-catalyzed condensation of the desired thiol with the lactol. Both the C-10- α - and β -configured thiol ethers were synthesized with a view to making them available for the anticancer activity evaluation using a variety of cell lines. The results show that many of the synthetic derivatives studied possessed good potential as anticancer agents. In order to draw more information on the origin of the anticancer activity, one of the compounds (**9a**), that showed a broad-spectrum activity in terms of reducing the viability of most of the cell lines studied, in particular proven to be most effective against Prostate (PC-3) cells, was studied in detail to find the underlying mechanism of its action by MTT assay, immunoblotting, flow cytometry and microscopy. Pretreatment of the PC-3 cells with *N*-acetyl cysteine affected the efficacy of **9a**, suggesting the role of reactive oxygen species in reducing their viability. Cell cycle analysis showed increase in G1 phase that was indicative of G1 cell cycle arrest. Wound healing assay revealed anti-migratory effect of **9a**. Quantitative PCR and western blot analysis showed changes in the gene expression of PCNA, E2F1, Pin1, cyclinD1, phospho-c-jun, c-Myc, eIF4E and other genes involved in proliferation and maintaining the transformed phenotype of prostate cancer cells. Here we report the anti-proliferative property of **9a** with a vital and potent target(s) in prostate cancer cells with one of such targets being Pin1

belonging to the parvulin family of PPIases. The results suggest that **9a** could be a promising agent in combating prostate cancer.

Keywords: Artemisinin thioacetal; *S*-Linked dihydroartemisinin; Anticancer activity; Pin1

1. INTRODUCTION

Artemisinin (**1**, ART, see Fig.1 below) and its derivatives (artemisinins, ARTs) have been a set of extremely successful drugs used for combating malaria, in particular, resistant malaria [1]. Some of the important attributes of ARTs such as their high efficacy, quick action, and minimum side effects have greatly influenced researchers around the globe prompting them to study their pharmacological properties beyond the antimalarial activity. Thus, anti-helminthic, antifungal, antiviral as well as anticancer activities are some of the other reported properties of ARTs [2]. Since the anticancer action of ART-related endoperoxides was reported in the early 1990s by Woerdenbag et al [3], a number of ARTs have been developed in attempts to derive the best-desired effect against cancer cells.

The anticancer effects of ARTs have been found to be majorly associated with ROS (reactive oxygen species) production following cleavage of the endoperoxide moiety present in their ring system which gets reduced by the ferrous ions present inside the cancer cells in the high amount owing to the need for rapid proliferation [[4], [5], [6], [7]]. But the debate on the exclusivity of this mode of anticancer mechanism got started seriously when ROS-independent apoptosis in HL-60 leukemia cells was reported by Lu et al [8], followed later by Qin et al in Hep G2 cells by artesunate [9]. These and other reports suggest unequivocally that ARTs affect a spectrum of pathways involved in proliferation, metastasis, and apoptosis [[10], [11], [12], [13]]. Thus, the versatility of ART and its derivatives indicated above led us to the synthesis and anticancer screening of a library of novel sulfur-linked ARTs as reported herein.

In the current study, we used *S*-linked artemisinin derivatives (**4a-13b**) to study their anti-cancer property on seven cancer cell lines (LNCaP, PC-3, A-431, HeLa, Hep G2, MDA-MB-231, and A549). Addition of sulfur atom aids in the enhanced uptake of molecules [14], and this may enhance the anti-cancer property of these derivatives. In our study, we found **5b** and **9a** affecting more than 50% cell viability against most of the cell lines studied. Thus, for a further mechanistic study on the mode of action of this class of compounds, compound **9a** was chosen. It

was found in this study that **9a** inhibited cell proliferation, affected/influenced the colony formation nature and induced apoptosis in metastatic PC-3 cells.

Further, in our study, we discovered that the compound had vital targets, Pin1 being one of them, which importantly is a pleiotropic effector, having a number of interacting partners influencing a number of signaling cascades including cell proliferation and apoptosis. Pin1 is a small enzyme known for catalyzing the *cis-trans* isomerization of proteins phosphorylated on serine or threonine, at the proline amide bond, thereby altering the conformation and consequently regulating the protein function [[15], [16]]. Subsequent studies reported in the literature highlighted the role of Pin1 in various cancers, in which either it is overexpressed and or over activated [[17], [18]]. A clinical study on prostate cancer patients has demonstrated Pin1 as an independent prognostic marker [19]. Although ART derivatives have been shown to inhibit cancer cell proliferation including prostate cancer cells, there are no reports of any ART derivative inhibiting prostate cancer cell proliferation involving Pin1. In the present study using **9a**, we have shown the apoptosis of metastatic prostate cancer cell line PC-3 with the down-regulation of Pin1 at the protein level.

2. RESULTS AND DISCUSSION

Chemistry. Fishwick et al described that dihydroartemisinin (**2**, DHA) was responsible for the inhibition of neurite outgrowth from differentiating NB2a neuroblastoma cells. Subsequent studies confirmed the cytotoxic effects towards neurons [20]. It is well known that ART derivatives bearing an alkyl group, as in artemether (**2a**), arteether (**2b**), etc, at C-10 through oxygen-linkage are readily turned over by cytochrome P-450 present in the liver to produce **2** that has been proven to be neurotoxic (Fig.1) [21]. The elimination half-life of the water-soluble **2** is less than 1 h after intravenous administration in rats [22]. Therefore, we wished to synthesize derivatives of artemisinin that are potentially more stable to cytochrome P-450. *S*-Linked residues at C-10 of artemisinin seemed to serve this purpose. This derivative may also emerge as relatively more stable to hydrolysis. Moreover, additional substituent groups can also be introduced in the residue to change the solubility characteristics of the compound derived.

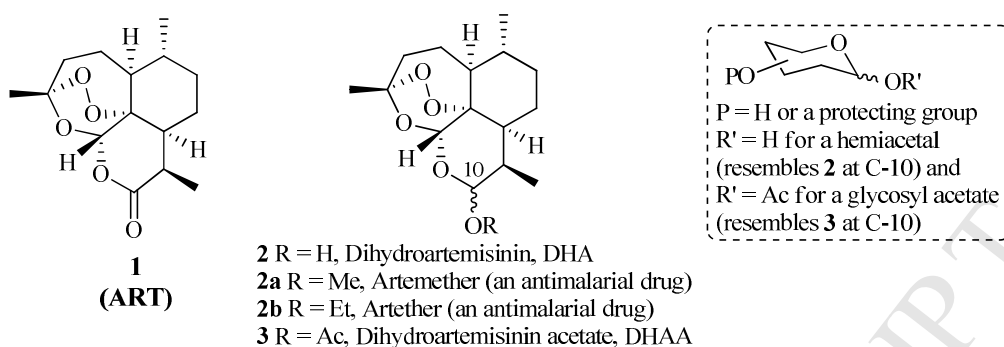
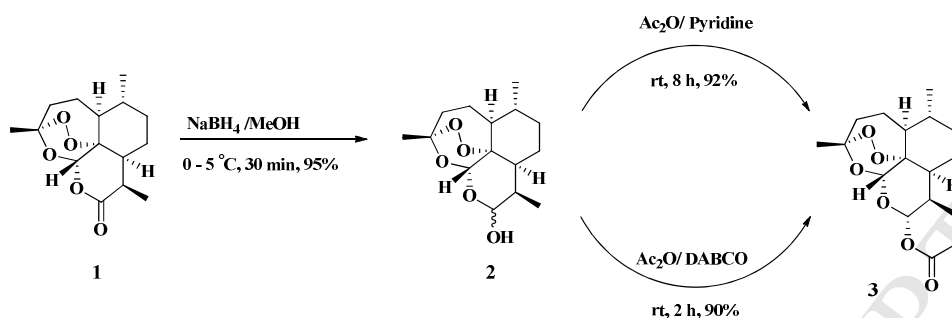


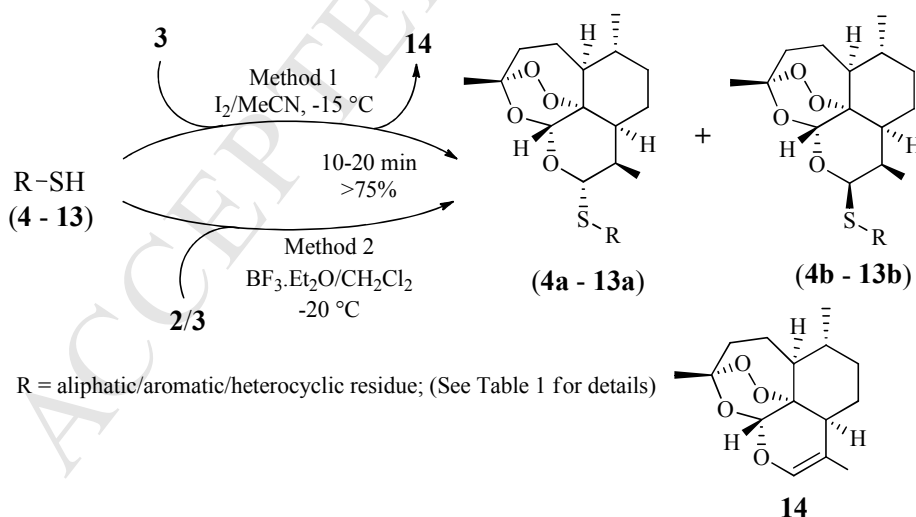
Fig. 1. Artemisinin (**1**) and some of its known derivatives **2** & **3**. In the inset is shown the anomeric center of a pyranosugar for comparison of the C-10 center of **2** & **3**

For the synthesis of novel *S*-linked artemisinins, DHA (**2**) was used as the starting material. Reduction of the commercially available ART (**1**) with sodium borohydride in dry methanol at 0 °C afforded an equilibrium mixture of α and β isomers of **2** in 30 min in 95% yield as shown in Scheme 1a. The stereochemistry of **2** [23], at C-10 was determined by ^1H and ^{13}C NMR spectroscopy. The signals for the C-10- α - and β -hydrogens appeared at 4.75 ppm ($J = 9.2$ Hz) and 5.30 ppm ($J = 3.2$ Hz) respectively. Presence of the hydroxyl group was confirmed by absorption at 3369 cm^{-1} in the IR spectrum and further confirmation of the product was obtained by MS (MALDI-TOF) for $\text{C}_{15}\text{H}_{24}\text{O}_5$, calculated m/z 284.16. Found m/z 307.65 $[\text{M}+\text{Na}]^+$, 323.65 $[\text{M}+\text{K}]^+$. The lactol **2** thus obtained was then acetylated using acetic anhydride as the acyl donor in the presence of pyridine (8 h, rt), or alternatively, DABCO (2 h, rt), as the acyl transfer agent. The lactol acetate **3** was obtained as its α - isomer in excellent yield the structure of which was, again, proven by NMR spectral characterization as for **2**. Thus, compared to a value of 4.75 ppm in **2**, the H-10 signal shifted downfield (5.78 ppm, $J = 9.9$ Hz) in the case of **3**. Moreover, in the ^{13}C NMR spectrum of **3**, the carbonyl carbon appeared at 169.9 ppm. In its IR spectra, likewise, the 1752 cm^{-1} absorption obtained was also typical for the carbonyl group. The MS spectrum of the compound (MALDI-TOF: for $\text{C}_{17}\text{H}_{26}\text{O}_6$, calculated m/z 326.17; found m/z 349.51 $[\text{M}+\text{Na}]^+$, 365.59 $[\text{M}+\text{K}]^+$) was also confirmatory of the expected acetate's structure.



Scheme 1a. Synthesis of dihydroartemisinin and dihydroartemisinin acetate

An examination of the nature of the lactol residue in **2**/the lactol acetate residue in **3**, readily reveals their resemblance to the anomeric center of a pyranosugar, as its hemiacetal/the derived glycosyl acetate, respectively (please see the structure shown inset under (Fig.1) for a general representation of this feature). Therefore it could not be surprising that when **3** was treated with an alkyl thiol in the presence of molecular iodine, a method that is used for the synthesis of alkyl thioglycosides of sugars from their respective per-*O*-acetylated glycoses [24], the desired lactol thioether was successfully obtained in excellent yields (Method 1, Scheme 1b). In the same manner, treatment of **3**, with alkyl thiols in the presence of $\text{BF}_3 \cdot \text{Et}_2\text{O}$ [25], a traditional Lewis acid employed for the electrophilic activation of the glycosyl acetate residue for *S*-glycosylation, also led to the formation of the expected lactol thioethers (Method 2, Scheme 1b).



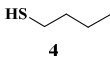
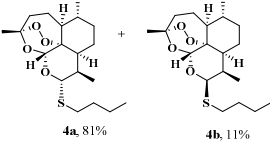
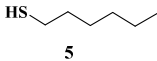
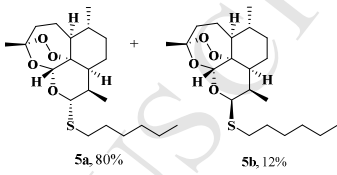
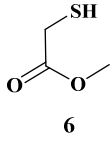
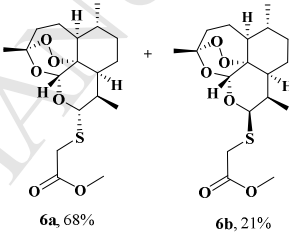
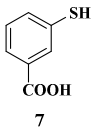
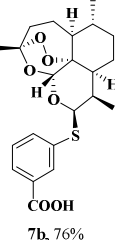
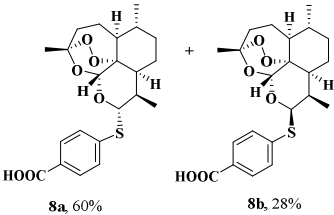
Scheme 1b. Synthesis of various thioethers of DHA

In the case of the BF_3 -catalyzed reaction it was observed that a significant quantity of the β -product accompanied the major α -compound formed in the reaction. They could be separated

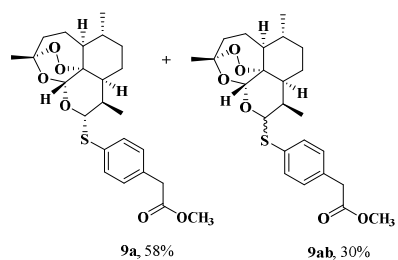
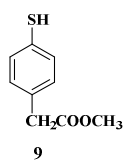
chromatographically on a column of silica for their unambiguous characterization by various spectroscopic techniques. The stereochemistry of the products was ascertained by the H-10 chemical shift observed in their respective ^1H NMR spectra. The large coupling constant between H-9 and H-10 was indicative of *trans*-diaxial relationship and was assigned the α -configuration (**4a** in the case of *n*-BuSH), while the small coupling constant was indicative of *cis* relationship and was assigned the β -configuration. Interestingly, in the case of the iodine-catalyzed reaction of **3** with alkane thiols, an exclusive formation of the α -configured product could be achieved. Thus in a model reaction when DHAA taken up in MeCN was treated with *n*-BuSH (**4**, entry 1, Table 1) at $-15\text{ }^\circ\text{C}$ the desired *S*-butyl derivative **4a** was obtained in a yield of 75% in 15 min of reaction. The isomer **4a** was the only product obtained under the above conditions when a 4 mol equiv of the thiol was used for the reaction. In the presence of lower mol equiv of the thiol, the corresponding β -isomer **4b** was also obtained along with **4a**. Thus, under the conditions of DHAA:*n*-BuSH of 1:1, **4a**:**4b** was obtained in a ratio of approximately 1:1 whereas at a DHAA:*n*-BuSH ratio of 1:2, the set of isomeric compounds were obtained in a ratio of 3:2. It was also observed that the iodine-method was best suited for alkyl thiols such as **4** and **5**. In the case of *N*-containing thiol acceptors such as **12**, **13**, etc the reaction did not take place at $-15\text{ }^\circ\text{C}$. But when it was attempted at room temperature, was found to lead to the formation of degradation products such as the anhydro compound (**14** [26], Scheme 1b). Thus, although the iodine-catalyzed method described above was well-suited for the preparation of α -*S*-alkyl-linked artemisinin derivatives, the $\text{BF}_3\cdot\text{Et}_2\text{O}$ -assisted method was finally adopted in the current context in view of its wider applicability as well as the requirement for both the α - and β -linked compounds for the biological evaluation later.

Based on the above-described method various *S*-linked compounds, **4a** [27], **4b** [27], **5a**, **5b**, **6a**, **6b**, **7b**, **8a**, **8b** [28], **9a**, **9ab**, **10a**, **10b**, **11a**, **12a**, **12b**, **13a** and **13b** were obtained by using thiols **4**, **5**, **6**, **7**, **8**, **9**, **10**, **11**, **12** and **13**, respectively, as the starting materials as shown in Table 1; and were characterized by standard spectroscopic techniques as described in the foregoing.

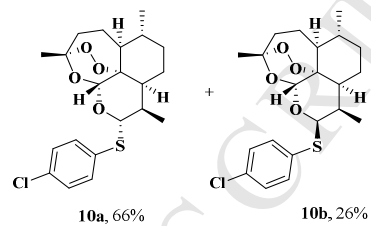
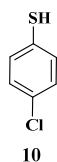
Table 1. S-Linked artemisinin derivatives synthesized having aliphatic/aromatic/heterocyclic substitution at C-10 position

Entry	R ₂ -SH	Products
1	 <p>4</p>	 <p>4a, 81% 4b, 11%</p>
2	 <p>5</p>	 <p>5a, 80% 5b, 12%</p>
3	 <p>6</p>	 <p>6a, 68% 6b, 21%</p>
4	 <p>7</p>	 <p>7b, 76%</p>
5	 <p>8</p>	 <p>8a, 60% 8b, 28%</p>

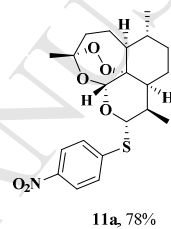
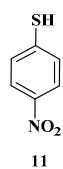
6



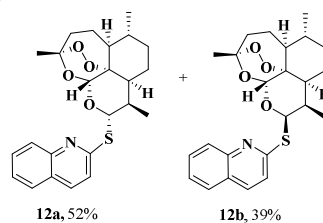
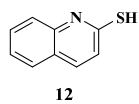
7



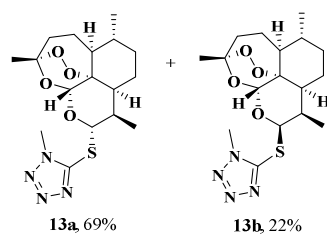
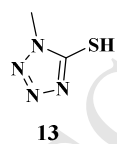
8



9



10



Computational study. Various pharmacokinetic parameters of the synthesized derivatives were examined by ADMET study. The results revealed that the synthesized compounds possess the drug-likeness properties governed by the Lipinski's rule of five. The LogP values, that denotes the hydrophilicity/lipophilicity of compounds, are in the permissible range for the synthesized compounds as shown in Table 2. As low hydrophilicity leads to a high logP value and vice versa, governing the absorption or permeation of compounds, a logP value lower than 5 is a good indicator for the absorption property of compounds. The numbers of HB donor and HB acceptor in the molecule are the other important parameters for an expected better absorption and permeation of compounds that also turned out to be in the allowed range for the synthesized compounds. In addition, the synthesized compounds fell under 500 daltons in their molecular weight, within the recommended limits (by the Lipinski's rule) showing them to be acceptable in terms of the solubility/cell membrane permeability parameters.

Table 2. Drug likeness property calculated using Qikprop software.

Entry	ADME descriptors	Molecular weight	HB Donor	HB Acceptor	logPo/w
	Standard Range	<500 Da	(< 5)	(< 10)	(< 5)
1	Arteether	312.40	0	5.65	2.82
2	Artemether	298.37	0	5.65	2.36
3	Artemisinin	282.33	0	5.25	1.73
4	4a	356.51	0	4.45	4.00
5	4b	356.51	0	4.45	3.8
6	5a	384.57	0	4.45	4.78
7	5b	384.57	0	4.45	4.51
8	6a	372.47	0	6.45	3.03
9	6b	372.47	0	6.45	2.9
10	7b	420.52	1	6.45	3.90
11	8a	420.52	1	6.45	3.87
12	8b	420.52	1	6.45	3.52
13	9a	448.57	0	6.45	4.65
14	9ab	448.57	0	6.45	4.09

15	10a	410.95	0	4.45	5.12
16	10b	410.95	0	4.45	4.93
17	11a	421.50	0	5.45	3.87
18	12a	427.55	0	4.95	5.24
19	12b	427.55	0	4.95	5.01
20	13a	382.47	0	6.95	2.54
21	13b	382.47	0	6.95	2.39

The aqueous solubility of a compound is important in determining its absorption and distribution properties, usually indicated as LogS value of the compounds (Table 3). On this count also, the synthesized compounds exhibited their respective values in the permissible range. Central nervous system (CNS) activity parameter for any compound allows the range from -2 to +2. A value of -2 for a compound is considered as inactive and a value of +2 as active. As shown in Table 3 our compounds have CNS score ranging from -1 to 2. Out of these compounds, two have shown a score of +2 and therefore these two compounds, namely **10a** and **10b**, could be CNS-toxic. Similarly values of other parameters like apparent Caco-2 cell permeability, blood-brain barrier (logBB), apparent MDCK permeability, skin permeability (logKp) and serum-protein binding (logKhsa) are also in the acceptable range for synthesized compounds (Table 3).

Table 3. Pharmacokinetic parameters calculated using Qikprop Software

Entry	ADME descriptors	Predicted CNS activity	logS for aqueous solubility	Apparent Caco-2 permeability (nm/sec)	logBB for Brain/Blood	Apparent MDCK permeability (nm/sec)	logKp for skin permeability	logKhsa Serum Protein Binding
	Standard Range	(-2,+2)	(-6.5/0.5)	(<25 poor, >500 great)	(-3/1.2)	(<25 poor, >500 great)	(-8/-1)	(-1.5/1.5)
1	Arteether	1	-3.08	5875.74	0.24	3354.40	-1.76	-0.11
2	Artemether	1	-2.44	5878.13	0.31	3355.88	-1.86	-0.27
3	Artemisinin	0	-2.26	1811.52	-0.31	940.29	-2.95	-0.32
4	4a	1	-3.91	6711.94	0.21	4800.64	-1.46	0.34
5	4b	1	-4.50	8538.22	0.29	6025.41	-1.26	0.33
6	5a	1	-4.82	6712.21	0.08	4800.85	-1.27	0.60

7	5b	1	-5.3	8455.58	0.16	6000.93	-1.07	0.54
8	6a	0	-4.04	1885.35	-0.23	1439.10	-2.63	0.01
9	6b	0	-3.87	1712.89	-0.27	1273.34	-2.71	-0.03
10	7b	-1	-4.40	209.13	-0.46	173.99	-2.99	0.27
11	8a	-1	-4.91	185.07	-0.59	165.60	-3.03	0.24
12	8b	-1	4.56	166.73	-0.65	129.76	-3.16	0.13
13	9a	0	-5.69	2640	-0.17	2189.78	-1.92	0.58
14	9ab	0	-4.20	2116.63	-0.18	1665.76	-2.09	0.36
15	10a	2	-5.51	8539.19	0.64	10000	-1.04	0.68
16	10b	2	-5.22	6511.72	0.53	10000	-1.29	0.64
17	11a	0	-4.78	1022.69	-0.44	784.24	-2.78	0.45
18	12a	1	-5.77	6977.64	0.38	6360.93	-0.85	0.80
19	12b	1	-5.30	5726.85	0.30	4942.01	-1.04	0.73
20	13a	0	-3.13	1781.75	-0.12	1395.80	-2.75	-0.18
21	13b	0	-3.07	1298.90	-0.24	971.88	-3.02	-0.21

[#]Schrodinger Release 2014-1: QikProp, Schrodinger, LLC, New York, NY, 2014

Biology. The compounds thus synthesized (Table 1) were evaluated for their anticancer potential (as pure α - and β -isomers and/ their 1:1 mixture, as applicable). For the evaluation of the compounds, the cell viability MTT assay was conducted using the following cancer cell lines, namely LNCaP & PC-3 (prostate cancer cell lines), A-431 (epidermoid carcinoma cell line), HeLa (cervical cancer cell line), Hep G2 (hepato-carcinoma cell line), MDA-MB-231 (breast cancer cell line) & A549 (Lung cancer cell line) and the percentage cell viability of the synthesized *S*-Linked artemisinin derivatives was calculated and is shown in Table 4. Further, 12 of the above compounds, namely, **4b**, **5a**, **5b**, **7b**, **8a**, **8b**, **9a**, **9ab**, **10a**, **10b**, **11a** and **12b** showed less than 50% cell viability on LNCaP cell line. Likewise, thirteen of them, namely, **4b**, **5b**, **6a**, **6b**, **8b**, **9a**, **9ab**, **7b**, **11a**, **12a**, **12b** and **13a**, **13b**, showed less than 50% cell viability on PC-3 cell line. In the same manner, while compounds **4b**, **5a**, **5b**, **8b**, **9a**, **10a**, **10b**, **11a**, and **12b** were active against on A-431 cell line, compounds **4b**, **5a**, **5b**, **9a**, **9ab**, **10a**, **10b** and **11a** were active

against HeLa cells; compounds **5a**, **5b**, **8b**, **9a**, **10a** and **10b** were active against Hep G2 cells; and compounds **5b** and **9a** were active against MDA-MB-231 as depicted in (Fig. S1 A and B). Significantly, these compounds, as can be seen from Table 4, were only marginally active, if at all, in A549 cell line. Following the encouraging results obtained in the above screening experiments, the IC₅₀ values for **5b** and **9a** were calculated for four different cell lines and the results are shown in Table 5. The significant reduction in the cell viability of various cell lines at 10 μM with these derivatives can be seen from the results, which is in sharp contrast to that of artemisinin that requires > 200 μM concentration to be effective as reported earlier against different cancer cell lines [[29], [30], [31]].

Table 4. Percentage cell viability of different cancer cell lines against synthesized S-linked artemisinin derivatives

Entry	Compound	LNCaP	PC-3	A-431	HeLa	Hep G2	MDA-MB-231	A549
1	Control	100±5.0	100±18.8	100±11.7	100±11.5	100±6.5	100±20.0	100±9.6
2	4a	90±11.4	92±4.7	86±21.9	82±11.8	92±5.8	90±4.1	96±5.6
3	4b	47±1.7	33±3.9	47±13.3	49±4.0	52±2.2	71±20.5	79±7.6
4	5a	36±2.1	90±2.9	35±9.0	44±4.1	35±0.8	72±13.3	70±5.3
5	5b	46±4.4	39±3.0	45±4.0	49±2.8	41±5.6	39±6.6	55±6.1
6	6a	60±9.7	32±2.4	75±12.0	79±4.7	80±5.5	98±4.6	91±5.7
7	6b	71±2.4	44±9.9	77±17.4	80±10.6	94±3.0	99±4.3	97±3.4
8	7b	43±2.2	41±5.7	90±8.9	58±5.0	60±8.7	97±7.0	89±3.0
9	8a	47±5.1	84±2.3	58±10.5	60±3.0	64±5.1	95±13.2	79±6.0
10	8b	41±1.9	32±3.2	31±6.2	55±10.1	45±3.5	64±13.1	76±3.2
11	9a	38±2.7	28±5.1	35±5.4	43±3.2	50±2.2	45±4.8	68±3.1
12	9ab	31±1.0	31±15.8	52±12.7	43±3.9	67±7.9	96±6.4	74±6.3
13	10a	37±2.3	70±13.4	42±6.6	48±5.0	42±1.2	97±8.1	55±10.5
14	10b	37±4.3	99±2.1	36±7.2	41±2.7	36±1.7	70±15.9	52±6.0

15	11a	46±1.2	50±10.7	44±11.6	50±10.0	56±3.5	98±3.9	70±7.1
16	12a	77±20.7	33±5.0	93±6.5	87±4.9	96±2.4	90±12.1	100±7.1
17	12b	41±1.2	39±3.4	44±4.5	63±6.8	72±7.2	78±17.1	87±3.4
18	13a	78±4.1	47±7.7	87±14.4	95±9.2	95±5.7	75±27.2	89±4.3
19	13b	97±5.3	28±2.8	97±7.5	93±8.4	93±6.4	86±18.8	100±3.8

LNCaP, PC-3 (prostate cancer cell lines), A-431 (epidermoid carcinoma cell line), HeLa (cervical cancer cell line), Hep G2 (hepato-carcinoma cell line), MDA-MB-231 (breast cancer cell line), A549 (Lung cancer cell line).

Table 5. IC₅₀ values for the *S*-linked artemisinin derivatives **5b** and **9a** against different cancer cell lines (μM)

Compounds	PC3	A431	Hep G2	MDA-MB-231
5b	5.8	3.99	10.72	3.94
9a	6.13	13.3	6.08	9.03

Results of the primary screening thus proved compounds **5b** and **9a** to be of comparable broad-spectrum anticancer activity effective on six (namely, LNCaP, PC-3, A-431, HeLa, HepG2, and MDA-MB-231) of the seven cancer cell lines evaluated. Thus, based on the fact that the synthetic protocol was consistently α -stereoselective, making the preparation of crystalline **9a** in the required quantities extremely facile, compound **9a** was chosen for further detailed studies using the prostate cancer cell line PC-3 (against which they had the best activity with IC₅₀ of 6.13 μM) as the cell line of choice. The efficacy of **9a** was also compared with natural artemisinin (ART) on the PC-3 cells by the MTT assay and results so obtained proved the superiority of **9a** as can be seen from (Fig. 3 A). The results obtained on the effect of compound **9a**, as a function of concentration (0.1, 0.3, 1.0, 3 and 10 μM) and treatment time (24, 48 and 72 h), on the viability of PC-3 cells as evaluated by MTT assay are shown in (Fig. 3 B-D). Thus, a treatment time of 24 h had no significant effect on the viability even up to 10 μM. Concentrations of 1 to 10 μM, however, showed a significant effect when treated for 72 h.

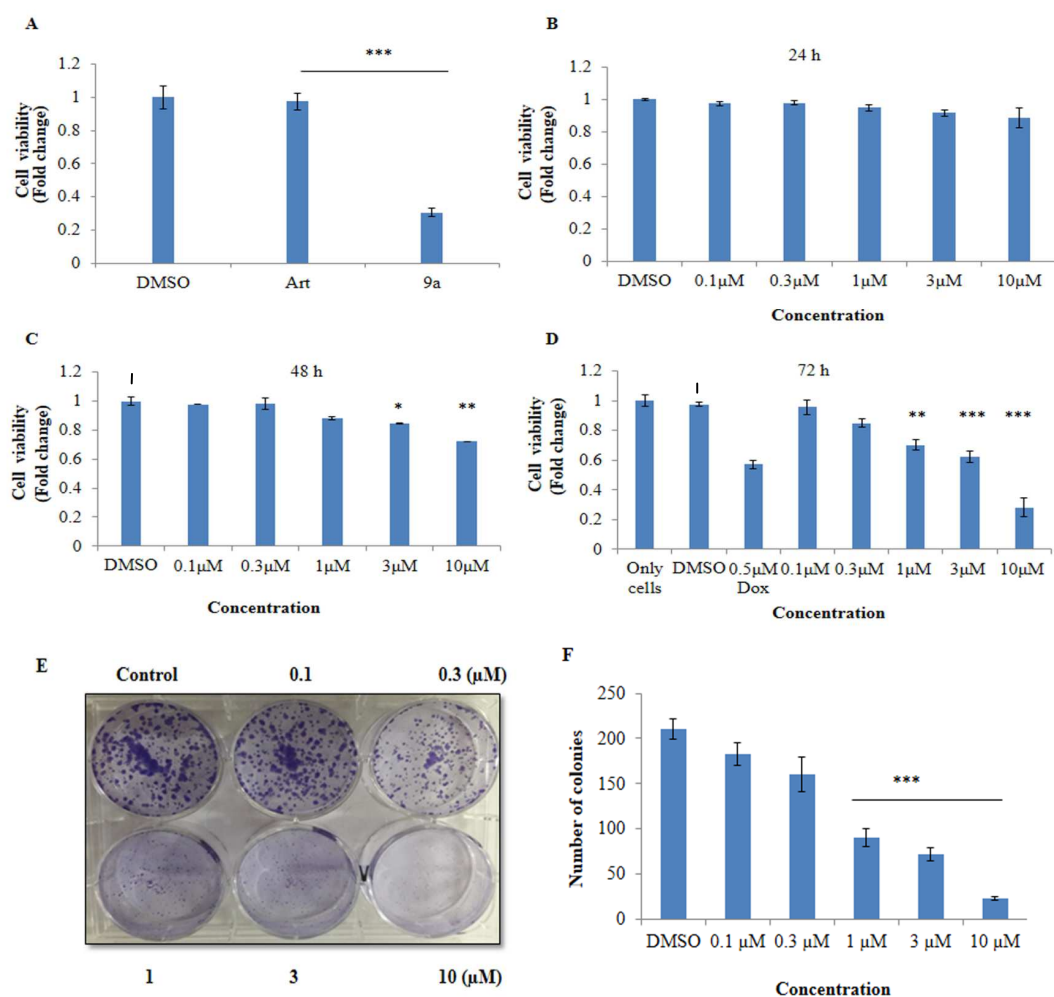


Fig. 2. Reduction of the viability and cell proliferation of prostate cancer (PC-3) cells by compound **9a**: **(A)** Efficacy of **9a** compared with artemisinin against treated PC-3 cells at 10 μ M for 72 h. **(B, C and D)** PC-3 cells was treated with **9a** in time (24, 48 and 72 h) and dose dependent manner and assayed, post-incubation, with MTT reagent for the cell viability. DMSO and doxorubicin (Dox)-exposed cells were used as a vehicle and positive control group respectively. **(E)** Representative image of the colony formation assay. **(F)** Bar graph showing the colony numbers in each treated group, as analyzed by Image J software. Results are expressed as fold change \pm s. d. and are representative of three separate experiments each performed in quadruple. (*) indicates $P \leq 0.05$ and (**) indicates $P \leq 0.01$ and (***) indicates $P \leq 0.001$ - significant difference, control Vs respective treatment group..

For evaluating the long-term cell survival and the ability of the cells to form colonies in the presence of **9a**, and for comparison, separately with artemisinin (at 3 and 10 μ M), colony assay was performed in a dose-dependent manner. The outcome of experiment was in accordance with the results obtained in the MTT assay and thus, while a reduced clonogenic growth was observed

in a dose-dependent manner with **9a** (as shown in Fig. 2 E and F), a much less effect was observed with artemisinin even at 10 μ M concentration (Fig. S 2A). Both of these assays proved that the anti-proliferative activity of **9a** is significantly higher than that of artemisinin itself against the PC-3 cells. As reported by Li. *et al.* the introduction of the sulfur atom in compounds, besides other possible factors, may have led to the enhancement of the cellular uptake, which may magnify the effect of compounds by accumulating around the target proteins [14].

For investigating the mechanism, lying behind the antiproliferative activity of this compound (**9a**) and to know whether ROS, if produced by the compound-treated cells, has any role in reducing the cell proliferation (as the anti-proliferative properties of artemisinin derivatives have been reported to be both ROS-dependent [[7], [13], [32]] and ROS-independent). We measured ROS level inside the cells following treatment of the cells with compound **9a** and performed fluorescence microscopy, with CM-H2DCFDA staining. A gradual increase of ROS producing cells on treatment with **9a**, as compared to the vehicle control cells, was observed as shown in (Fig. 3 A and B). Next the cells were pretreated with ROS scavenger NAC (20 μ M) for 2 h followed by treating them with **9a** for 72 h. The cytotoxicity of **9a** in the presence and absence of NAC was evaluated by MTT assay and it was found that the anti-proliferative property of **9a** significantly depended upon the ROS activity as shown in (Fig. 3 C). One of direct consequences of the abrupt increase in the ROS level is the alteration of mitochondrial membrane potential [33]. Thus, we next evaluated $\Delta\Psi_m$ using JC-1 probe and found a decreasing red/green ratio in the **9a**-treated cells as compared to the control as shown in (Fig. 3 D), which is a sign of early stage of apoptosis. In contrast, a nearly equal red/green ratio was observed for the artemisinin-treated cells (Fig. S 2B). Taken together, these experiments thus revealed a significant production as well as involvement of the ROS in the antiproliferative activity of compound **9a**.

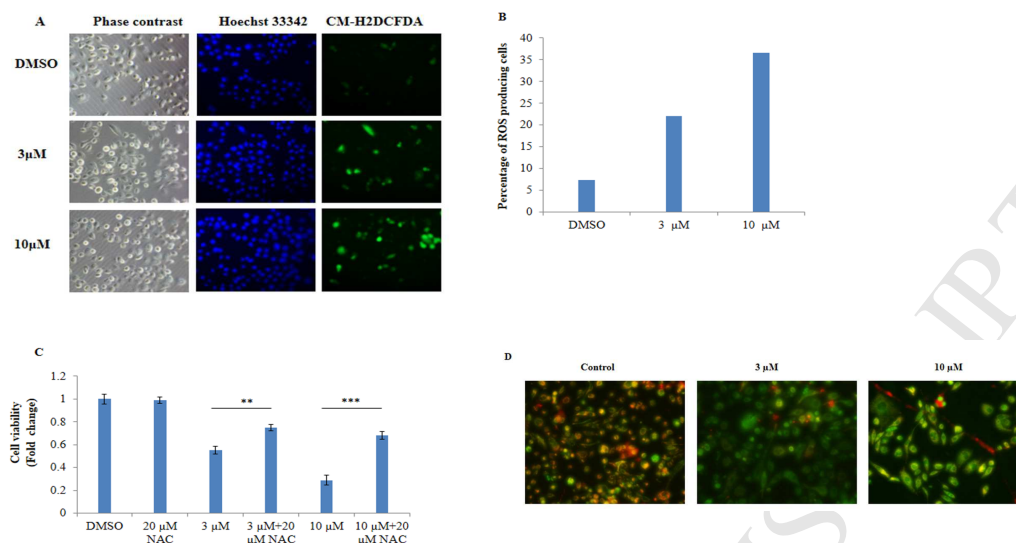


Fig. 3. (A) Representative photographs are shown for CM-H2DCFDA-stained PC-3 cells observed using fluorescence microscopy. (B) Bar graph showing the percentage of ROS producing cells for the representative image in (A). Involvement of ROS in the anti-proliferative activity of compound **9a**: (C) PC-3 cells were treated with **9a** at 3 and 10 μM alone and in the presence of the ROS scavenger NAC to explore the participation of any ROS activity and graph shows the cell viability of **9a**-treated cells in the presence of 20 μM NAC. Results are expressed as fold change ± s.d. and are representative of three separate experiments; (**) indicates $P \leq 0.01$ and (***) indicates $P \leq 0.001$. (D) $\Delta\Psi_m$ was evaluated using JC-1 dye by observing change in red/green fluorescence under fluorescence microscope.

We recalled, a study on the prostate cancer cells, including PC-3 cells, had found the existence of an inherent oxidative stress in these cells, for proliferation and survival [34], and a disproportional increase in the ROS level could lead to the cell cycle arrest and apoptosis [35]. Therefore, we next sought to check the status of different phases of the cell cycle and apoptosis in the **9a**-treated cells in the following sets of experiments. Cell cycle analysis revealed that PC-3 cells treated with 3 and 10 μM of **9a** were arrested in the G1 phase (54.49% and 53%) as compared to the control (42%) and was found to be consistent with the decrease in the percentage of cell population in S and G2M phase as shown in (Fig. 4 A, B and C). On the other hand treatment with 3 and 10 μM of artemisinin had a non-significant effect on the G1 phase and showing a 2 and 6 %, respectively, arrest in the S-phase of cell cycle (Fig. S 2C). Thus, the result so obtained in the cell cycle analysis led us to envisage the induction of apoptosis if any as to establish a link between the losses of viability via cell cycle arrest. So firstly, phase contrast microscopy was performed in order to detect any changes associated with apoptosis. As shown

in Fig.5 A, the images thus captured showed shrinkage in the cell size, which is one of the features associated with the early process of apoptosis. In contrast, the artemisinin-treated cells barely lost their cellular morphology (Fig. S 2D). Next, Hoechst 33342 staining and fluorescence microscopy were also carried out to assess any changes in the nuclear morphology, such as the nuclear condensation or nuclear fragmentation of the treated cells. It was found that the nuclei of the treated cells were condensed as compared to the vehicle control cells, as shown in (Fig. 5 B) as well as the artemisinin-treated cells (Fig. S 2D). To further confirm the induction of apoptosis following the treatment of cells for 72 h in a dose-dependent manner, caspase-9 and caspase-3 activation were checked by western blot. A decrease in the pro-caspase form of caspase 9 and 3, (Fig. 5 C), was found which further strengthened the finding of apoptosis pathway and the cause of reduction in the viability of **9a**-treated cells. This decrease in the pro-caspase 9 and 3 was accompanied by the down-regulation of the anti-apoptotic protein Bcl-xL and up-regulation of pro-apoptotic protein Bax in a dose-dependent manner, as shown in (Fig. 5 C), suggesting the activation of an intrinsic pathway following the treatment with **9a**. The down-regulation of Bcl-xL is a promising indicator for the future, as Bcl-xL is overexpressed in ~100% of the hormone-refractory prostate cancers and is associated with advanced disease, poor prognosis, recurrence, and metastasis [[36], [37]]. Finally, the cells treated with **9a** at 3 and 10 μ M levels of concentration were stained with propidium iodide to examine the cell death following apoptosis. Compound **9a** at these concentration levels significantly activated cell death in a dose-dependent manner following a 72 h-treatment, as shown in (Fig. 5 D and E). However, it may be noted that the maximum cell death observed was only 28.9%, approximately, in repeated experiments.

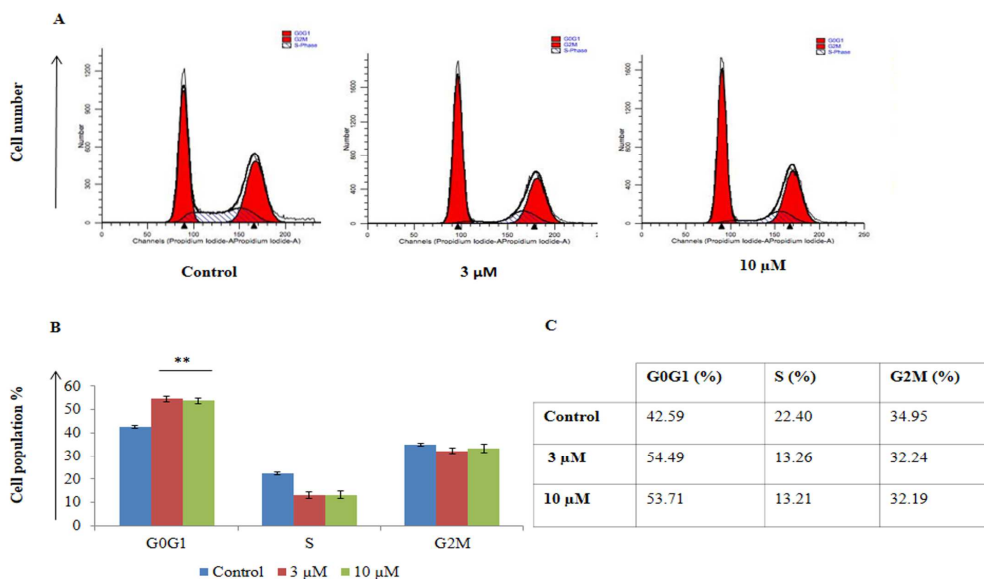


Fig. 4. 9a causes G1 cell cycle arrest in PC-3 cells (A, B) - Cells treated with 3 and 10 μ M of 9a were fixed and permeabilized with 80% chilled ethanol and stored for overnight at 4 $^{\circ}$ C. Then cells were washed and subjected to RNase treatment and PI staining for 30 min at room temperature for flow cytometry to analyze DNA content. (A) Histogram of a representative experiment. (B) Data are represented as mean \pm SD of three independent experiments, where (**) indicates $P < 0.01$ compared to vehicle control as determined by t-test. (C) Table showing percentage of cells in different phases of cell cycle following treatment with 9a as compared to control.

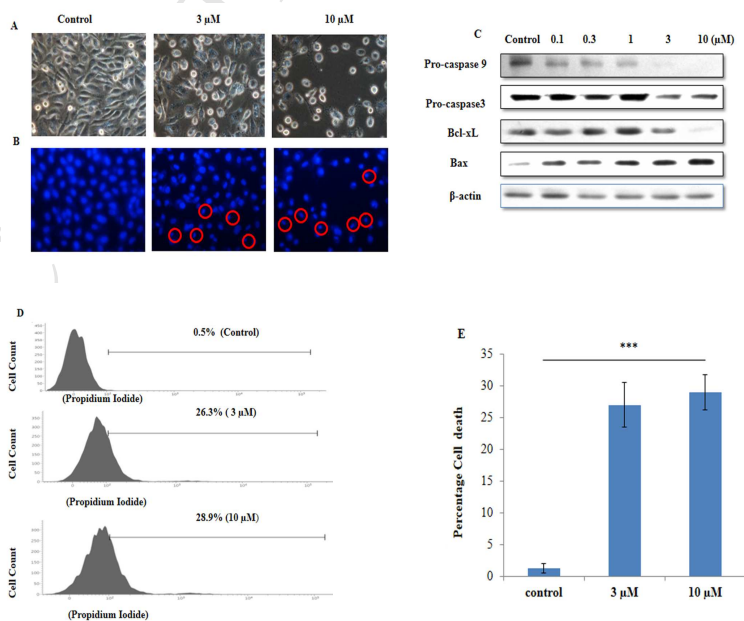


Fig. 5. 9a-Induced apoptosis and cell death in PC-3 Cells: (A) Morphology alteration in treated cells. Exponentially growing PC-3 cells were exposed to **9a** at 3 and 10 μM levels of concentration for 72 h, gently washed with $1\times\text{PBS}$ and then photographed with phase contrast microscopy. (B) Fluorescence micrographs of PC-3 prostate cancer cells stained with Hoechst 33342. Cells were treated with 3 and 10 μM solutions of **9a** for 72 h. It shows that **9a** induces apoptosis in PC-3 cells and are characterized by nuclear condensation. (C) PC-3 cells treated with **9a** for 72 h shows a decreased pro-form of caspases 9 and 3, the initiator and executioner caspases, and inhibition of the anti-apoptotic protein Bcl-xL whereas upregulation of pro-apoptotic Bax. (D) Cell death analysis after treatment with **9a**. PC-3 cells were cultured in a six-well culture plate, incubated with concentrations of 3 and 10 μM of **9a** for 72 h. Cells were harvested, washed with PBS and incubated with propidium iodide for 20 min at 4°C . Samples were acquired for cell death using flow cytometry. Cells with DMSO treatment were taken as the control. Data represent percentage cell death after treatment with different concentrations of compound **9a**. (E) Bar graph showing the percentage of cell death for the representative image in (D), where (***) indicates $-p < 0.001$ compared to vehicle control as determined by t-test.

Next, besides the apoptotic effect of **9a** against the PC-3 cells, we performed the scratch assay to assess the migration potential of these highly metastatic PC-3 cell lines following treatment with **9a** at 3 and 10 μM . As expected, we found that **9a** significantly inhibited migration of the PC-3 cells as compared to the control (Fig. 6 A and B). Contrary to this the artemisinin-treated cells retained the migration ability and filled the wound at the same time point as filled by the control group (Fig. S 2E). In addition, the anti-migration effect of **9a** was also assessed in the presence of pan caspase inhibitor Z-Vad-Fmk to inhibit any apoptotic process during the wound healing assay. It was found that blocking of apoptosis did not affect the anti migration effect of **9a** (Fig 6 C and D). Thus both of these experiments suggest that **9a** can inhibit PC-3 cell migration independent of its apoptotic effect. In connection with this inhibitory action of **9a** on the migration potential of PC-3 cells, Gelatin zymography was done to assess the level of gelatinases like MMP-2 and MMP-9 following treatment with **9a** at 3 and 10 μM levels. While a dose-dependent inhibition in the activity of MMP-9 was observed, MMP-2 remained unaffected as shown in (Fig. 6 E). MMPs are matrix metalloproteinases and are involved in matrix degradation that lead to cell migration causing metastasis and invasion [38]. In the context of prostate cancer, MMP-2 and MMP-9 have been reported to be associated with metastatic potential leading to severity of malignancy [39]. Therefore, the inhibition of MMP-9 by **9a** calls for further detailed study for evaluating its anti-metastatic potential against PC-3 cells.

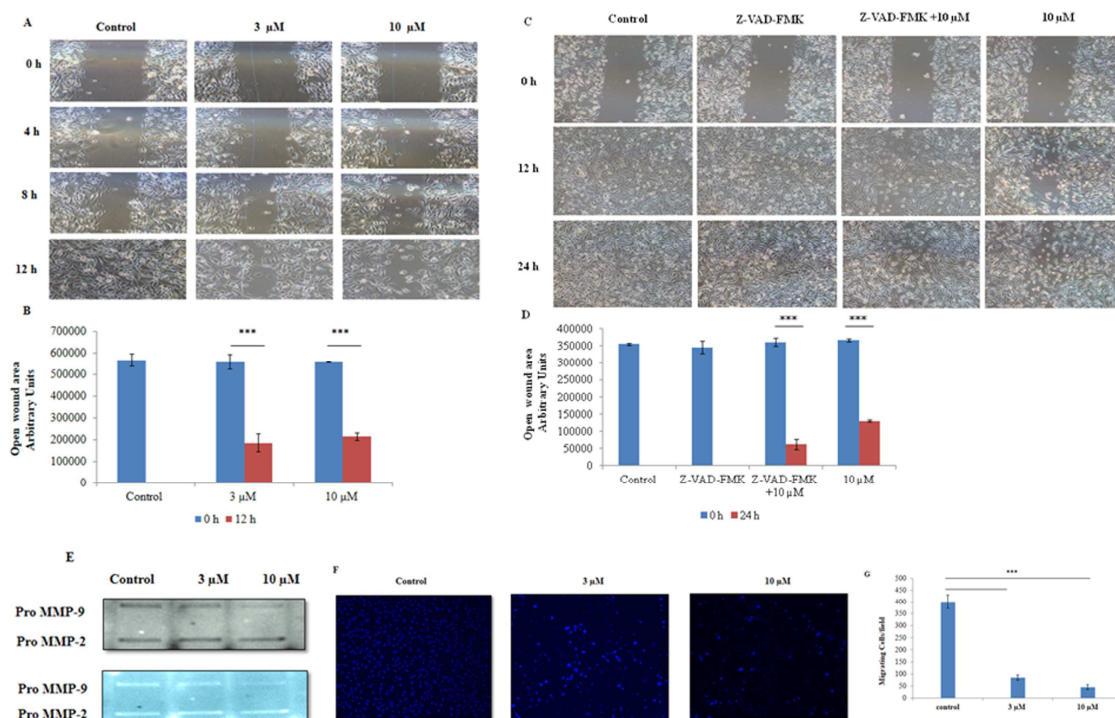


Fig. 6. 9a-Inhibited cell migration of PC-3 cells: **(A and B)** The inhibitory effect of **9a** on PC-3 cells migration detected using wound healing assay as shown in the representative image. Treatment with 3 and 10 μ M **9a** resulted in decreased cell migration of PC-3 cells as compared to DMSO treated group. A distinguishable difference was observed on the migration ability of PC-3 cells under the influence of **9a** at different time intervals (0, 4, 8 and 12 h) as evident from phase contrast micrographs. **(C and D) Wound healing assay** in the presence of pan caspase inhibitor Z-Vad-Fmk- cells were pretreated with Z-Vad-Fmk(10 μ M) for 2 h followed by treatment with **9a**, wound at 0, 12 and 24, are shown. **E Gelatin zymography**- Effect of **9a** on MMPs abundance and activity in serum-free media following treatment of PC-3 cells with 3 and 10 μ M concentrations. Briefly, post treatment of cells in serum-containing media for 48 h cells were further kept for 24 h in serum-free media. Media was collected and electrophoresed with gelatin (4mg/mL) for the analysis of MMP 9 and 2. Representative gelatinase zymograph, detected as white bands against blue background as well as black bands against grey background of repeated independent experiments, each of which showed similar results. **(F and G) Transwell assay** the inhibitory effect of **9a** on PC-3 cells migration detected using Transwell assay as shown in the representative images. Hoechst 33342 stained nuclei present number of migrating cells in control and respective treatments. Treatment with 3 and 10 μ M **9a** resulted in decreased cell migration of PC-3 cells as compared to DMSO treated group. Bar graph showing migrating cells/field. (***) indicates $-p < 0.001$ compared to vehicle control as determined by t-test.

Migration potential of PC-3 was also challenged by Transwell assay in the presence of 3 and 10 μM of **9a** and similar results were obtained as in scratch assay. The number of cells migrating through pores significantly decreased at both concentrations of **9a** as shown in (Fig. 6 F and G).

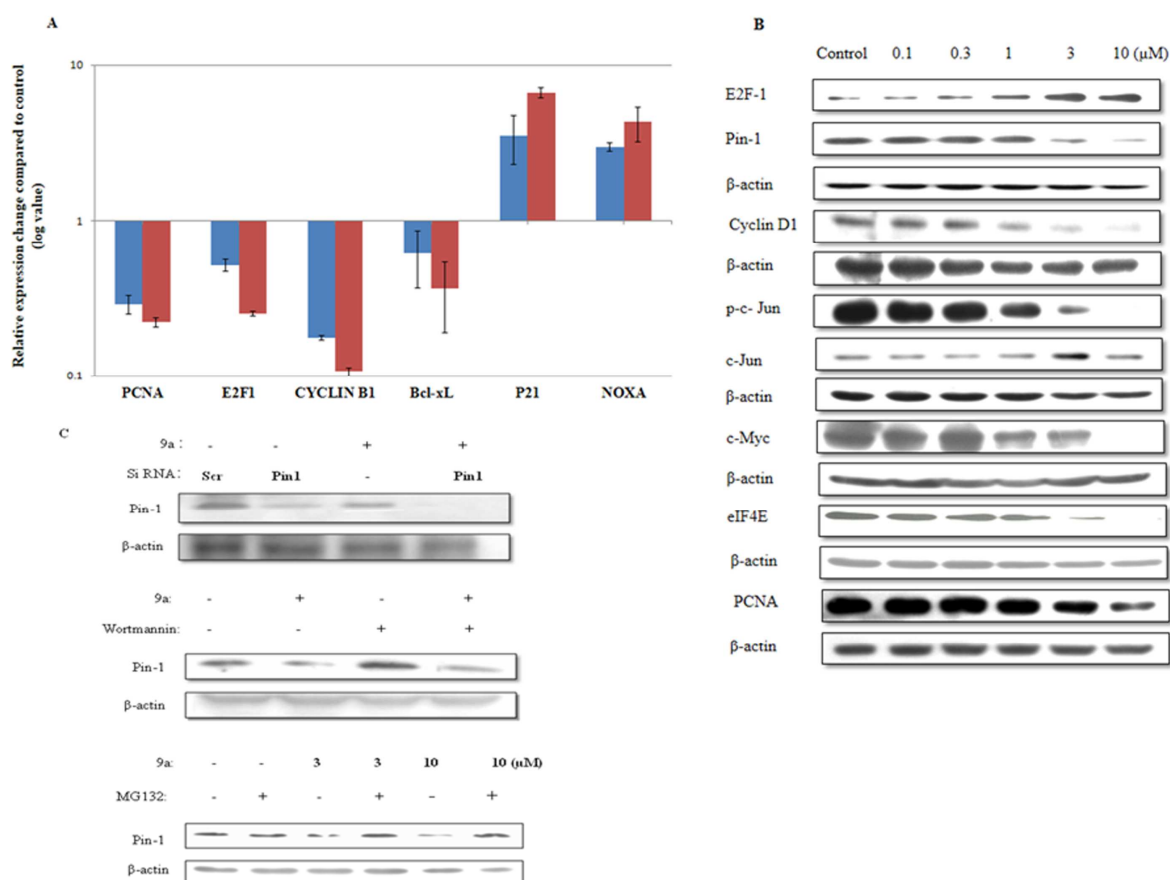


Fig. 7. (A) Effect of **9a** on mRNA expression evaluated by RT-PCR- A relative expression of PCNA, E2F1, Cyclin B1, Bcl-xL, p21 and Noxa at mRNA level following treatment of PC-3 Cells for 72 h at 3 μM (blue bar) and 10 μM (red bar) concentrations. Results are expressed as means \pm s.d. and are representative of three different experiments. (B) **9a** upregulates E2F1 whereas it inhibits Pin 1, Cyclin D1, phospho-c-jun, eIF4E, c-Myc and PCNA: PC-3 cells treated with (0.1-10 μM) of **9a** for 72 h were subjected to western blotting and β -actin was used as loading control. (C) Pin1 siRNA and **9a** together significantly down-regulated Pin1. PC-3 cells were transfected with Pin1-siRNA alone and with **9a** for 72 h and were subjected to western blotting and β -actin was used as loading control. Wortmannin, an autophagy inhibitor, unaltered the Pin1 inhibition by **9a**: PC-3 cells treated with 10 μM of

9a in the presence and absence of Wortmannin for 72 h were subjected to western blotting. Pretreatment with MG132 rescued Pin1 inhibition by **9a**.

Further, to study the mechanism responsible for the reduction observed in the viability of cells following treatment with **9a**, a set of genes (not shown) involved in cell division, apoptosis and anti-apoptotic processes were chosen and the following experiments were carried out. Towards this end, essentially, the mRNA expression analysis by real-time PCR was performed. Cells treated for 72 h with 3 μ M and 10 μ M concentrations of **9a** were analyzed for the changes in the mRNA level of the following genes – E2F1, PCNA, CyclinB1, Bcl-XL that were found to be down-regulated, and p21 and Noxa, that were found up-regulated, as shown in (Fig. 7 A). Only marginal changes in other selected genes were observed. E2F1 belonging to the E2F family of transcription factors act as a transcriptional activator for progression through the G1/S transition [40]. Activated E2F1 can induce apoptosis as well depending on the cumulative signal operating in the cell [41]. Here we have found the inhibition of E2F1 at transcript level using **9a** at 3 and 10 μ M levels but the upregulation at protein level in a dose-dependent manner as shown in (Fig. 7 A and B, respectively). This negative correlation between mRNA and protein abundance could exist due to the difference in the rate of protein synthesis and degradation for a given protein [42]. Thus it could be deduced that the up-regulation of E2F1 by **9a** steers the PC-3 cells towards apoptosis by modulating apoptotic signals.

Real-time analysis paved the way for further mechanistic study in which either the proteins of these mRNA or their targets were analyzed by western blotting. Pin1 is one of the E2F1 target genes [43], that has been found aberrantly upregulated or overactivated in many cancers and in prostate cancer it has been reported as an independent prognostic marker [19]. In our study, Pin1 was significantly down regulated at 3 μ M and 10 μ M of **9a** as shown in Fig. 7 B even with the up-regulation of E2F1, which indicates Pin1 as a target of **9a** independent of the requirement of E2F1 down-regulation. However, notably, the Pin 1 expression remained unaffected in the artemisinin-treated PC-3 cells (Fig. S 2F). The inhibition of Pin1 thus observed prompted us to evaluate cyclin D1 level, as an overexpression of the latter has been linked to the progression and development of cancer [44], as well as the fact that overexpression of Pin1 increases the cellular cyclin D1 levels and the activation of its promoter [[45], [46]]. Indeed we found that a down-regulation of cyclin D1 at the protein level occurred in a dose-dependent manner as depicted in (Fig. 7 B) with the inhibition of Pin1. This finding correlated well with a previous finding where

the loss of Pin1 function in mouse mimicked the cyclin-D1-null phenotypes [47]. Moreover, expression of cyclin D1 is also under the control of phosphorylated c-Jun [48]. Therefore we next sought to check the expression of the phosphorylated c-Jun, which is one of the interacting partners of Pin1 and also the transcription factor, for a number of genes involved in proliferation, including cyclin D1 [[49], [50], [51]] . Indeed, it was found inhibited significantly at both the concentration levels (3 μ M and 10 μ M) as shown in (Fig. 7 B). Thus, the modulation of E2F1/Pin1/Phospho-c-Jun/cyclin D1 suggests the possible mechanism by which **9a** is able to inhibit proliferation of prostate cancer PC-3 cells.

In parallel with the inhibition of the above mentioned proliferating signals, the expression of PCNA, a vital histologic marker for the G1/S phase in the cell cycle and whose expression level has been suggested for an early diagnosis of prostate cancer [52], was examined by real-time PCR as well as by western blot analysis. Indeed, it was found inhibited at both the transcript as well as the protein levels in a dose-dependent manner as shown in (Fig. 7 B). With the previous reports on other artemisinin derivatives such as DHA and artesunate down-regulating the c-Myc expression [[53], [54]] in other cancer cell lines, we investigated the expression of c-Myc, another proliferation regulator whose over expression is also one of the earliest molecular alterations in prostate cancer [55]. c-Myc is a transcription regulator for many cell proliferation genes including eIF4E [56], and the latter a component of mRNA 5' cap binding protein complex has been reported for aberrant expression in many cancers [57]. Both c-Myc and eIF4E are oncogenes and have been reported to exhibit a cooperation in an E μ -Myc transgenic model, contributing to aggressive lymphomagenesis and leading to chemotherapy resistance [58]. Down-regulation of c-Myc led us to check the expression of eIF4E and it was indeed found inhibited at 3 and 10 μ M of **9a** as shown in (Fig. 7 B). Moreover, the down-regulation of cyclin D1 could also be the consequence of inhibition of both c-Myc and eIF4E by **9a** as the expression of cyclin D1 has been reported to be eIF4E [56] as well as c-Myc-dependent [59].

In addition, we found the up regulation, at the transcript level as shown in (Fig. 7 A), of p21(WAF1/Cip1) that functions as an effector of multiple anti-proliferative signals and acting in both p53-dependent and p53-independent pathways and is mostly controlled at the transcription level [60]. In our study, we found a significant up-regulation of p21 mRNA, which shows that **9a** up-regulates the level of p21 in p53 null PC-3 cells by some mechanism independent of p53. In addition, we also found a significant down-regulation of cyclin B1 at the mRNA level which

could be a consequence of the p21 up-regulation, as p21 checks the expression of cyclin B1 in p53-dependent and independent ways by inhibiting CDK2 [[61], [62]]. The up-regulation of p21 at mRNA level and the down-regulation of PCNA at both the mRNA and the protein levels suggest a strong anti-proliferative effect of **9a** on the PC-3 cells as p21 competes for PCNA binding with DNA polymerase δ and inhibits the DNA synthesis [63]. Investigating the apoptotic effect of this derivative, a dose-dependent decrease of pro-caspase 9 and pro-caspase 3 was observed as shown in Fig. 5 C, and in search of changes in another apoptotic marker, we found an up-regulation of the pro-apoptotic Noxa at transcript level as in Fig. 7 A. Noxa is a BH3 only protein known to activate pro-apoptotic Bak and Bax [64], and indeed we found an upregulation of Bax at the protein level as in Fig. 5 C. On the other hand Noxa promotes the anti-apoptotic Mcl-1 degradation [65], and although we did not check Noxa at the protein level, a study on prostate cancer PC-3 cells treated with BH3 mimetic (-)-gossypol found an increase in the Noxa protein without a significant change of the mRNA level [66]. In our study, we found a dose-dependent increase in mRNA level of Noxa, which suggests an upregulation of Noxa protein, and involvement in the apoptotic pathway.

We carried out siRNA-mediated knockdown of Pin1, alone and in the presence of **9a**, and evaluated the expression of Pin1 by western blotting. The level of Pin1 was significantly down-regulated when the cells were treated with both the siRNA and Pin1 as compared to Pin1, siRNA or **9a** alone, as can be seen from Fig. 7 C, further showing that **9a** inhibited Pin1. To further validate Pin1 as one of the targets of **9a**, PC-3 cells were pre-treated for 2 h with Wortmannin (200 nM) and then with 10 μ M of **9a** for 72 h. Following incubation, the cell lysate was prepared and subjected to western blotting to check the inhibition of Pin1 in the presence of autophagy inhibitor Wortmannin. In the presence of Wortmannin with **9a** absent, the Pin1 level was found to be augmented whereas in the presence of both Wortmannin and **9a**, it was found to be down-regulated as in Fig. 7 C, which indicates that the inhibition of Pin1 is not autophagy-dependent but follows some other inhibitory mechanism induced by **9a**. This led us to investigate the proteasome-mediated inhibition of Pin1, if any. For this we assessed the **9a**-mediated inhibition of Pin1 in the presence of proteasome inhibitor MG132 (100 nM). Treatment with **9a** alone (3 and 10 μ M) reduced the expression of Pin1 whereas pretreatment with MG132 followed by treatment with **9a** rescued Pin1 inhibition (Fig. 7 C), which suggest that proteasomal

degradation of Pin1 is a predominant mode of its inhibition. In summary, the overall possible mode of action by compound **9a** is shown in Fig. 8.

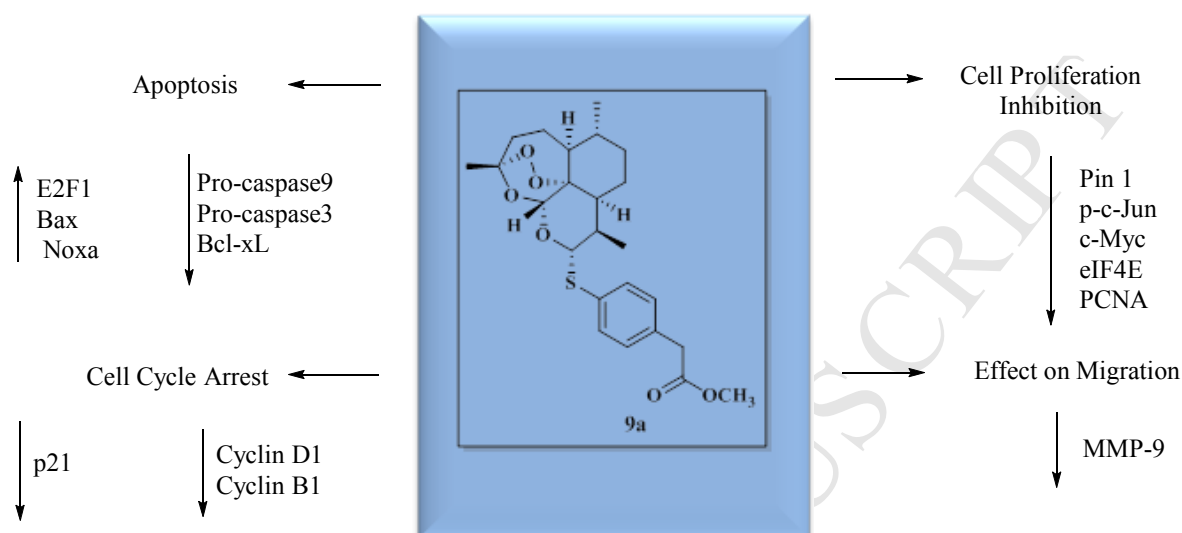


Fig. 8 Possible mode of action of compound **9a**

3. CONCLUSIONS

Efficient synthesis of a library of dihydroartemisinin thiolactol ethers has been achieved. Their structures were elucidated by standard spectroscopic techniques. It has been found that the iodine-mediated method for the preparation of this class of compounds is best suited when thiols to be used are alkane thiols, the *N*-containing thiols, in contrast, being less (or not at all) suitable for the purpose. It is, however, highly α -stereoselective and therefore holds good potential for application when the product desired is the neat α -thiolactol ether derivative. The $\text{BF}_3 \cdot \text{Et}_2\text{O}$ -mediated method is, on the other hand, more widely applicable and as a consequence a broad set of thiols can be used for the preparation of the corresponding thiolactol ether derivatives of dihydroartemisinin. The *S*-linked artemisinins reported in this work were proved highly effective against various cancer cell lines as evident from the MTT assay. Compound **9a** was chosen for further mechanistic study and was found to be exhibiting its action partly by generating ROS and partly by impairing the proliferating signals, thus affecting the cell viability of PC-3 cells and causing their arrest in G1 phase that may have lead to apoptosis by activating pro-caspase-9 and 3 and upregulating Bax and ultimately to the cell death. In the attempts made to elucidate its mode of action, it was found to be inhibiting Pin1, a pleiotropic regulator of various cellular

processes and has been found three- to four-fold higher in prostate cancer cell lines. In addition, we also found that the **9a**-treated PC-3 cells have an inhibiting effect on Pin1-interacting partners like cyclin D1, and phosphorylated-c-jun with parallel inhibition of c-Myc, eIF4E and PCNA which further quells the proliferation signals. Along with hampering the viability of PC-3 cells, **9a** was also found affecting the migration potential of these highly metastatic cells. In conclusion, this study presents the possible mechanisms by which artemisinin derivatives such as **9a** act as anti-proliferative, apoptotic as well as anti-metastatic agents for prostate metastatic PC-3 cancer cells.

4. EXPERIMENTAL SECTION

Materials and methods

All reagents and chemicals were purchased from Aldrich Chemical Co (Milwaukee, WI, USA) or Alfa Aesar (a Johnson Matthey Company). TLC analyses were performed on 0.2 mm Merck pre-coated silica gel 60 F₂₅₄ aluminum sheets and the spots were visualized under UV lamp and/or by immersion in an ethanolic solution of sulphuric acid (5%, v/v) followed by heating. Final purification was performed using silica gel 200-400 mesh size. Melting points were determined on a Buchi melting point (B-540) apparatus and are uncorrected. Specific rotations were recorded on a Rudolph Autopol IV Polarimeter. NMR spectra were recorded on a Bruker Avance DPX (400 MHz) spectrometer. ¹H NMR and ¹³C NMR spectra were referenced to the internal standard tetramethylsilane, in the respective deuterated solvents. Coupling constants (*J*) are reported in Hertz. All assignments were confirmed with the aid of two-dimensional ¹H-¹H (COSY) and/or ¹H-¹³C (HSQC) experiments using standard pulse programs. Processing of the spectra was performed with Topspin software. IR spectra were recorded on a Nicolet FT-IR Impact 410 instrument either as a thin film (neat) or as KBr pellet. Mass spectra were recorded on MALDI (Bruker Daltonics, Ultraflex TOF/TOF) spectrometer and High-resolution mass spectra (HRMS) on a Bruker Maxis spectrometer.

Dihydroartemisinin (**2**) [23]

Artemisinin (**1**, 2.0 g, 0.007 mol) was taken in distilled methanol (20 mL) and was cooled over an ice bath to 0-5 °C. To the solution, an excess of sodium-borohydride was added in small

portions during a period of 30 min. The solution was left to be stirred for 45 min at 0-5 °C after which TLC (EtOAc/Hexane, 1:3) showed completion of the reaction. After that, it was neutralized by 5% cold AcOH/water to get a white precipitate of dihydroartemisinin (**2**). White crystalline solid (yield, 1.91 g, 95%); IR (Neat) ν_{\max} 3369, 2924, 2854, 1446, 1377, 1174, 1134, 1092, 983, 875, 845, 783 cm^{-1} ; ^1H NMR (400 MHz, CDCl_3) δ_{H} 5.60 (s, 1H, β *H*-12), 5.39 (s, 1H, α *H*-12), 5.30 (d, 1H, $J = 3.2$ Hz, β *H*-10), 4.75 (d, 1H, $J = 9.2$ Hz, α *H*-10), 2.66-2.60 (m, 3H, OH, β *H*-9), 2.42-2.29 (m, 3H, α *H*-9, α/β *H*-4_{a1}), 2.07-2.01 (m, 2H, α/β *H*-4_{a2}), 1.95-1.75 (m, 4H, α/β *H*-5_{a1}, β *H*-8_{a1}, β *H*-8_{a2}), 1.72-1.63 (m, 3H, α *H*-8_{a1}, α/β *H*-7_{a1}), 1.58-1.46 (m, 4H, α/β *H*-8_a, α/β *H*-5_{a2}), 1.44, 1.43 (2s, 6H, α/β *H*-14), 1.39-1.29 (m, 4H, α *H*-8_{a2}, α/β *H*-6, β *H*-5_a), 1.25-1.22 (m, 1H, α *H*-5_a), 1.05-0.94 (m, 14H, α/β *H*-7_{a2}, α/β *H*-15, α/β *H*-16); ^{13}C NMR (100 MHz, CDCl_3) δ_{C} 104.39, 104.13 (α/β *C*-3), 96.42, 94.63, 91.20, 87.77 (α/β *C*-12, α/β *C*-10), 81.12, 80.36 (α/β *C*-12_a), 52.48, 51.52 (α/β *C*-5_a), 45.42, 44.30 (α/β *C*-8_a), 37.48, 37.37 (α/β *C*-6), 36.35, 36.26 (α/β *C*-4), 34.79, 34.69 (α/β *C*-7), 34.19, 30.77 (α/β *C*-9), 26.07, 25.97 (α/β *C*-14), 24.71, 24.66 (α/β *C*-5), 24.57, 22.13 (α/β *C*-8), 20.38, 20.25 (α/β *C*-15), 13.19, 12.72 (α/β *C*-16); MS (MALDI-TOF) for $\text{C}_{15}\text{H}_{24}\text{O}_5$, calculated m/z 284.16. Found m/z 307.65 [$\text{M}+\text{Na}$] $^+$, 323.65 [$\text{M}+\text{K}$] $^+$.

Dihydroartemisinin acetate (**3**) [23]

Method A: To a solution of dihydroartemisinin (**2**, 1.0 g, 3.5 mmol) in pyridine (12 mL) at room temperature was added acetic anhydride (8 mL) and the solution was left at room temperature for 8 h. Completion of the reaction was ascertained by TLC (EtOAc/hexane, 1:3). It was then co-evaporated thrice with toluene and was concentrated under reduced pressure. The resulting mixture taken up in CH_2Cl_2 was then successively washed, twice with cold dilute hydrochloric acid (5%), saturated sodium bicarbonate solution, and finally brine. The organic portion was collected and dried over anhydrous sodium sulfate and was then concentrated under reduced pressure to give product **3** (yield, 1.06 g, 92%).

Method B: To a solution of **2** (1.0 g, 3.5 mmol) in acetic anhydride (2 mL), DABCO (200 mg, 1.7 mmol) was added and the solution was stirred at room temperature. The reaction was complete after 2 h as evidenced by TLC (EtOAc: Hexane, 1:3). The resulting mixture was extracted with CH_2Cl_2 and was successively washed, thrice with cold dilute hydrochloric acid (5%), saturated sodium bicarbonate solution and finally with brine. The organic portion was

collected and after drying over anhydrous sodium sulfate and was concentrated under reduced pressure to give the product **3**. White crystalline solid (yield, 1.03 g, 90%); IR (Neat) ν_{\max} 2927, 2869, 2086, 1752, 1634, 1453, 1375, 1228, 1130, 1103, 1029, 918, 877, 848, 825 cm^{-1} ; ^1H NMR (400 MHz, CDCl_3) δ_{H} 5.78 (d, 1H, $J = 9.9$ Hz, $H-10$), 5.44 (s, 1H, $H-12$), 2.59-2.53 (m, 1H, $H-9$), 2.38 (dt, 1H, $J = 3.9$ Hz, $J = 14.5$ Hz, $J = 13.5$ Hz, $H-4a_1$), 2.13 (s, 3H, COCH_3), 2.08-2.00 (m, 1H, $H-4a_2$), 1.92-1.87 (m, 1H, $H-5a_1$), 1.80-1.69 (m, 2H, $H-8a_1$, $H-7a_1$), 1.65-1.59 (m, 1H, $H-8a$), 1.52-1.45 (m, 1H, $H-5a_2$), 1.44-1.40 (m, 4H, $H-14$, $H-6$), 1.38-1.32 (m, 1H, $H-8a_2$), 1.31-1.26 (m, 1H, $H-5a$), 1.06-0.98 (m, 1H, $H-7a_2$), 0.96 (d, 3H, $J = 6.0$ Hz, $H-16$), 0.85 (d, 3H, $J = 7.1$ Hz, $H-15$); ^{13}C NMR (100 MHz, CDCl_3) δ_{C} 169.86 (COCH_3), 104.68 ($C-3$), 91.85, 91.49 ($C-12$, $C-10$), 80.13 ($C-12a$), 51.55 ($C-5a$), 45.22 ($C-8a$), 37.27 ($C-6$), 36.20 ($C-4$), 34.07 ($C-7$), 31.76 ($C-9$), 25.99 ($C-14$), 24.57 ($C-5$), 21.99 ($C-8$), 21.15 ($C-15$), 20.23 (COCH_3), 12.09 ($C-16$); MS (MALDI-TOF) for $\text{C}_{17}\text{H}_{26}\text{O}_6$, calculated m/z 326.17. Found m/z 349.51 $[\text{M}+\text{Na}]^+$, 365.59 $[\text{M}+\text{K}]^+$.

General procedure for the synthesis of S-linked artemisinin derivatives having aliphatic/aromatic/heterocyclic substitution on the C-10 sulfur: 4a [27], 4b [27], 5a, 5b, 10a, 10b, 11a, 12a, 12b, 13a, 13b

To a solution of dihydroartemisinin (**2**, 500 mg, 1.76 mmol) in dry CH_2Cl_2 (10 mL) cooled to -20 $^\circ\text{C}$, the desired thiol (aliphatic/aromatic or heterocyclic substituted, 1.2 mol equiv) was added. $\text{BF}_3 \cdot \text{Et}_2\text{O}$ (0.22 mL, 1 mol equiv) was added after 5 min of holding the solution stirred at -20 $^\circ\text{C}$ and the stirring was continued at the same temperature until TLC showed the completion of the reaction (10 to 20 min). The reaction mixture was diluted with CH_2Cl_2 and was washed successively with saturated aqueous NaHCO_3 , ice-cold water, and brine. The organic layer was dried over anhydrous sodium sulfate and was then concentrated to dryness under reduced pressure. It was then chromatographed on silica gel column (230-400 mesh size) using EtOAc/Hex as the eluent. The respective product was characterized by standard physical methods.

General procedure for the synthesis of S-linked artemisinin derivatives having an aliphatic substitution on the C-10 sulfur: 4a,²⁷ 4b,²⁷ 5a, 5b

To a solution of dihydroartemisinin acetate (**3**, 500 mg, 1.53 mmol) in anhydrous MeCN (8 mL) at -15 °C, the desired aliphatic thiol (2-4 mol equiv) was added dropwise from a syringe. I₂ (0.5 mol equiv) was added after 5 min at -15 °C; and was stirred until TLC (EtOAc: Hex, 1:3) showed completion of the reaction (usually 15 min). The reaction mixture was then quenched with cold saturated aqueous sodium thiosulfate solution. The resulting mixture was extracted with CH₂Cl₂, was washed successively with saturated aqueous NaHCO₃, ice-cold water and brine, and the organic layer was dried over anhydrous sodium sulfate. Then it was concentrated under reduced pressure and was chromatographed on silica gel column (230-400 mesh size) using EtOAc/Hex as the eluent. Characterization of the isolated product by physical methods confirmed the respective structure.

General procedure for the synthesis of S-linked artemisinin derivatives using thiols bearing carboxylic acid/ester substituent groups: 6a, 6b, 9a, 9ab, 7b, 8a, 8b [28]

To a solution of dihydroartemisinin (**2**, 500 mg, 1.76 mmol) in dry CH₂Cl₂ held at -20 °C (10 mL), the desired thiol-bearing carboxylic/ester moiety (1.2 mol equiv) was added. BF₃.Et₂O (0.22 mL, 1 mol equiv) was then added to it after 5 min; and the stirring was continued until TLC (CH₂Cl₂/MeOH, 5%) showed completion of the reaction (10 to 20 min). The reaction mixture was extracted with CH₂Cl₂ and was washed thrice with ice-cold water. The organic layer was then dried over anhydrous sodium sulfate. It was then concentrated under reduced pressure to a small volume and was chromatographed on silica gel (230-400 mesh) column using CH₂Cl₂/MeOH as the eluent. Characterization of the isolated product by physical methods of analysis confirmed the respective structure.

The title compounds **4a** and **4b** were synthesized from 1-butanethiol (**4**).

10- α -S-Butyl-10-deoxoartemisinin (4a) [27]

Syrup (yield, 81%); [α]_D²⁴ -5.79° (c 1.0, CHCl₃); IR (Neat) ν_{\max} 2925, 1634, 1275, 1260, 1081, 749 cm⁻¹; ¹H NMR (400 MHz, CDCl₃) δ_{H} 5.28 (s, 1H, *H*-12), 4.52 (d, 1H, *J* = 10.8 Hz, *H*-10), 2.81-2.74 (m, 1H, *H*-1'a₁), 2.69-2.57 (m, 2H, *H*-1'a₂, *H*-9), 2.36 (dt, 1H, *J* = 4.0 Hz, *J* = 14.4 Hz, *J* = 13.6 Hz, *H*-4a₁), 2.04-1.98 (m, 1H, *H*-4a₂), 1.91-1.85 (m, 1H, *H*-5a₁), 1.75-1.56 (m, 5H, *H*-8, *H*-2', *H*-7a₁), 1.52-1.43 (m, 2H, *H*-8a, *H*-5a₂), 1.43 (s, 3H, *H*-14), 1.39-1.30 (m, 3H, *H*-6, *H*-3'), 1.28-1.23 (m, 1H, *H*-5a), 1.07-0.98 (m, 1H, *H*-7a₂), 0.95 (d, 3H, *J* = 6.3 Hz, *H*-16), 0.93-0.89 (m,

6H, *H*-15, *H*-4'); ^{13}C NMR (100 MHz, CDCl_3) δ_{C} 104.27 (*C*-3), 92.24 (*C*-12), 80.55 (*C*-10), 80.42 (*C*-12a), 51.76 (*C*-5a), 46.03 (*C*-8a), 37.36 (*C*-6), 36.25 (*C*-4), 34.06 (*C*-7), 31.91 (*C*-1'), 31.69 (*C*-9), 27.99 (*C*-2'), 25.94 (*C*-14), 24.74 (*C*-5), 22.14 (*C*-3'), 21.28 (*C*-8), 20.25 (*C*-15), 15.11 (*C*-16), 13.73 (*C*-4'); ESI-HRMS: m/z Calcd for $\text{C}_{19}\text{H}_{32}\text{NaO}_4\text{S}$ 379.1919. Found: 379.1914 $[\text{M}+\text{Na}]^+$.

10- β -S-Butyl-10-deoxoartemisinin (4b) [27]

Syrup (yield, 11%); $[\alpha]_{\text{D}}^{24} +68.25^\circ$ (c 1.0, CHCl_3); IR (Neat) ν_{max} 2917, 1275, 1260, 750 cm^{-1} ; ^1H NMR (400 MHz, CDCl_3) δ_{H} 5.62 (s, 1H, *H*-12), 5.27 (d, 1H, $J = 5.1$ Hz, *H*-10), 3.05-3.01 (m, 1H, *H*-9), 2.67 (t, 2H, $J = 6.9$ Hz, *H*-1'), 2.37 (dt, 1H, $J = 3.7$ Hz, $J = 13.7$ Hz, $J = 14.0$ Hz, *H*-4a₁), 2.04 (d, 1H, $J = 14.3$ Hz, *H*-4a₂), 1.89-1.79 (m, 2H, *H*-5a₁, *H*-8a₁), 1.72-1.63 (m, 2H, *H*-2'), 1.61-1.58 (m, 2H, *H*-8a₂, *H*-7a₁), 1.54-1.47 (m, 2H, *H*-8a, *H*-5a₂), 1.43-1.38 (m, 6H, *H*-14, *H*-6, *H*-3'), 1.28-1.24 (m, 1H, *H*-5a), 1.10-1.03 (m, 1H, *H*-7a₂), 0.96-0.93 (m, 6H, *H*-16, *H*-15), 0.91 (t, 3H, $J = 7.3$ Hz, *H*-4'); ^{13}C NMR (100 MHz, CDCl_3) δ_{C} 104.18 (*C*-3), 88.02 (*C*-12), 86.70 (*C*-10), 81.19 (*C*-12a), 52.67 (*C*-5a), 45.17 (*C*-8a), 37.19 (*C*-6), 36.41 (*C*-4), 34.41 (*C*-7), 32.38 (*C*-1'), 32.06 (*C*-2'), 31.80 (*C*-9), 26.18 (*C*-14), 24.60 (*C*-5), 24.35 (*C*-8), 22.04 (*C*-3') 20.33 (*C*-15), 14.85 (*C*-16) 13.73 (*C*-4'); ESI-HRMS: m/z Calcd for $\text{C}_{19}\text{H}_{32}\text{NaO}_4\text{S}$ 379.1919. Found: 379.1918 $[\text{M}+\text{Na}]^+$.

The title compounds **5a** and **5b** were synthesized from 1-hexanethiol (**5**).

10-Deoxo-10- α -S-(hexyl)-artemisinin (5a)

Syrup (yield, 80%); $[\alpha]_{\text{D}}^{24} -9.89^\circ$ (c 1.0, CHCl_3); IR (Neat) ν_{max} 2926, 2871, 1376, 1195, 1151, 1038, 928, 880, 829, 749 cm^{-1} ; ^1H NMR (400 MHz, CDCl_3) δ_{H} 5.28 (s, 1H, *H*-12), 4.52 (d, 1H, $J = 10.7$ Hz, *H*-10), 2.80-2.73 (m, 1H, *H*-1'a₁), 2.68-2.59 (m, 2H, *H*-1'a₂, *H*-9), 2.36 (dt, 1H, $J = 3.6$ Hz, $J = 13.3$ Hz, $J = 13.8$ Hz, *H*-4a₁), 2.01 (d, 1H, $J = 14.4$ Hz, *H*-4a₂), 1.89-1.85 (m, 1H, *H*-5a₁), 1.72-1.57 (m, 7H, *H*-8a₁, *H*-7a₁, *H*-2', *H*-3', *H*-8a), 1.52-1.41 (m, 5H, *H*-5a₂, *H*-6, *H*-14), 1.39-1.29 (m, 5H, *H*-4', *H*-8a₂, *H*-5'), 1.25-1.20 (m, 1H, *H*-5a), 1.07-1.01 (m, 1H, *H*-7a₂), 0.95 (d, 3H, $J = 6.3$ Hz, *H*-16), 0.92 (d, 3H, $J = 7.3$ Hz, *H*-15), 0.88 (t, 3H, $J = 6.2$ Hz, *H*-6'); ^{13}C NMR (100 MHz, CDCl_3) δ_{C} 104.26 (*C*-3), 92.25 (*C*-12), 80.56 (*C*-10), 80.42 (*C*-12a), 51.77 (*C*-5a), 46.03 (*C*-8a), 37.36 (*C*-6), 36.26 (*C*-4), 34.06 (*C*-7), 31.70 (*C*-9), 31.47 (*C*-1'), 29.81 (*C*-2'), 28.75 (*C*-3'), 28.34 (*C*-4'), 25.94 (*C*-14), 24.74 (*C*-5), 22.56 (*C*-5'), 21.28 (*C*-8), 20.25 (*C*-15),

15.11 (C-16), 14.06 (C-6'); ESI-HRMS: m/z Calcd for $C_{21}H_{36}NaO_4S$ 407.2232. Found: 407.2233 $[M+Na]^+$.

10-Deoxo-10- β -S-(hexyl)-artemisinin (5b)

Syrup (yield 12%); $[\alpha]_D^{24} +196.86^\circ$ (c 1.0, $CHCl_3$); IR (Neat) ν_{max} 2924, 1275, 1256, 1151, 1039, 750 cm^{-1} ; 1H NMR (400 MHz, $CDCl_3$) δ_H 5.61 (s, 1H, H-12), 5.27 (d, 1H, $J = 5.3$ Hz, H-10), 3.05-3.01 (m, 1H, H-9), 2.66 (t, 2H, $J = 7.0$ Hz, H-1'), 2.37 (dt, 1H, $J = 3.9$ Hz, $J = 14.0$ Hz, $J = 14.0$ Hz, H-4a₁), 2.07-2.01 (m, 1H, H-4a₂), 1.91-1.78 (m, 2H, H-5a₁, H-8a₁), 1.73-1.64 (m, 2H, H-2'), 1.62-1.56 (m, 2H, H-8a₂, H-7a₁), 1.53-1.46 (m, 2H, H-8a, H-5a₂), 1.43 (s, 3H, H-14), 1.42-1.35 (m, 3H, H-6, H-3'), 1.31-1.25 (m, 5H, H-4', H-5', H-5a), 0.99-0.91 (m, 7H, H-7a₂, H-16, H-15), 0.88 (t, 3H, $J = 6.7$ Hz, H-6'); ^{13}C NMR (100 MHz, $CDCl_3$) δ_C 104.18 (C-3), 88.01 (C-12), 86.69 (C-10), 81.20 (C-12a), 52.67 (C-5a), 45.17 (C-8a), 37.19 (C-6), 36.41 (C-4), 34.42 (C-7), 32.70 (C-1'), 32.06 (C-2'), 31.44 (C-9), 29.68 (C-3'), 28.60 (C-4'), 26.18 (C-14), 24.60 (C-5), 24.35 (C-8), 22.53 (C-5') 20.34 (C-15), 14.85 (C-16), 14.04 (C-6'); ESI-HRMS: m/z Calcd for $C_{21}H_{36}NaO_4S$ 407.2232. Found: 407.2231 $[M+Na]^+$.

10-Deoxo-10- α -S-(methoxycarbonylmethyl)-artemisinin (6a)

The title compound **6a** was synthesized from methyl thioglycolate (**6**) by the general procedure described above.

Syrup (yield, 68%); $[\alpha]_D^{24} -12.9^\circ$ (c 1.0, CH_2Cl_2); IR (Neat) ν_{max} 2926, 2872, 1738, 1435, 1377, 1280, 1195, 1129, 1037, 928, 879, 828 cm^{-1} ; 1H NMR (400 MHz, $CDCl_3$) δ_H 5.28 (s, 1H, H-12), 4.71 (d, 1H, $J = 10.9$ Hz, H-10), 3.73 (s, 3H, O- CH_3), 3.57 (d, 1H, $J = 15.0$ Hz, S- CH_2), 3.39 (d, 1H, $J = 15.1$ Hz, S- CH_2), 2.59-2.53 (m, 1H, H-9), 2.36 (dt, 1H, $J = 4.0$ Hz, $J = 14.4$ Hz, $J = 13.6$ Hz, H-4a₁), 2.04-1.98 (m, 1H, H-4a₂), 1.91-1.84 (m, 1H, H-5a₁), 1.75-1.68 (m, 2H, H-8), 1.62-1.56 (m, 1H, H-7a₁), 1.51-1.39 (m, 5H, H-8a, H-5a₂, H-14), 1.37-1.30 (m, 1H, H-6), 1.28-1.23 (m, 1H, H-5a), 1.08-0.99 (m, 1H, H-7a₁), 0.95 (d, 3H, $J = 6.2$ Hz, H-16), 0.92 (d, 3H, $J = 7.2$ Hz, H-15); ^{13}C NMR (100 MHz, $CDCl_3$) δ_C 171.26 (CO), 104.30 (C-3), 92.30 (C-12), 80.37 (C-10), 80.07 (C-12a), 52.35 (C-5a), 51.70 (OCH₃), 46.01 (C-8a), 37.28 (C-6), 36.18 (C-4), 33.96 (C-7), 32.11 (SCH₂), 30.15 (C-9), 25.91 (C-14), 24.69 (C-5), 21.23 (C-8), 20.21 (C-15), 14.67 (C-16); ESI-HRMS: m/z Calcd for $C_{18}H_{28}NaO_6S$ 395.1504. Found: 395.1504 $[M+Na]^+$.

10-Deoxo-10- β -S-(methoxycarbonylmethyl)-artemisinin (6b)

The title compound **6b** was synthesized from methyl thioglycolate (**6**) by the general procedure described above. Syrup (yield, 21%); $[\alpha]_D^{24} +96.9^\circ$ (c 1.0, CH₂Cl₂); IR (Neat) ν_{\max} 2926, 2872, 1738, 1435, 1377, 1280, 1195, 1129, 1037, 928, 879, 828 cm⁻¹; ¹H NMR (400 MHz, CDCl₃) δ_H 5.56 (s, 1H, *H*-12), 5.43 (d, 1H, *J* = 5.4 Hz, *H*-10), 3.73 (s, 3H, OCH₃), 3.49 (d, 1H, *J* = 15.2 Hz, SCH₂), 3.32 (d, 1H, *J* = 15.1 Hz, SCH₂), 3.08-3.03 (m, 1H, *H*-9), 2.36 (dt, 1H, *J* = 4.0 Hz, *J* = 13.6 Hz, *J* = 13.6 Hz, *H*-4a₁), 2.06-2.01 (m, 1H, *H*-4a₂), 1.91-1.84 (m, 1H, *H*-5a₁), 1.82-1.72 (m, 2H, *H*-8), 1.71-1.65 (m, 1H, *H*-7a₁), 1.54-1.45 (m, 2H, *H*-8a, *H*-5a₂), 1.44-1.34 (m, 4H, *H*-14, *H*-6), 1.29-1.26 (m, 1H, *H*-5a), 1.03-0.93 (m, 7H, *H*-7a₂, *H*-16, *H*-15); ¹³C NMR (100 MHz, CDCl₃) δ_C 171.27 (CO), 104.24 (C-3), 88.00 (C-12), 86.70 (C-10), 81.09 (C-12a), 52.59 (C-5a), 52.50 (OCH₃), 44.92 (C-8a), 37.15 (C-6), 36.30 (C-4), 34.35 (C-7), 33.71 (SCH₂) 31.92 (C-9), 26.05 (C-14), 24.54 (C-5), 24.37 (C-8), 20.29 (C-15), 14.48 (C-16); ESI-HRMS: *m/z* Calcd for C₁₈H₂₈NaO₆S 395.1504. Found: 395.1504 [M+Na]⁺.

The title compound **7b** was synthesized from 3-mercaptopbenzoic acid (**7**) by the general procedure described above.

10- β -S-[3'-(Carboxyphenyl)]-10-deoxoartemisinin (7b)

Colorless solid (yield, 76%); mp 73.3-76.2 °C; $[\alpha]_D^{24} +245.3^\circ$ (c 1.0, CH₂Cl₂); IR (Neat) ν_{\max} 3410, 2950, 2843, 2864, 2522, 2077, 1644, 1454, 1442, 1113, 1052, 1032, 1016, 932, 706 cm⁻¹; ¹H NMR (400 MHz, CDCl₃) δ_H 8.21 (s, 1H, *H*-2'), 7.95 (d, 1H, *J* = 7.9 Hz, *H*-4'), 7.82 (d, 1H, *J* = 7.7 Hz, *H*-6'), 7.41 (t, 1H, *J* = 7.8 Hz, *H*-5'), 5.74 (s, 1H, *H*-12), 5.63 (d, 1H, *J* = 5.2 Hz, *H*-10), 3.17-3.13 (m, 1H, *H*-9), 2.39 (dt, 1H, *J* = 3.4 Hz, *J* = 14.0 Hz, *J* = 13.8 Hz, *H*-4a₁), 2.06 (d, 1H, *J* = 14.3 Hz, *H*-4a₂), 1.92-1.89 (m, 1H, *H*-5a₁), 1.82-1.73 (m, 3H, *H*-8, *H*-7a₁), 1.59-1.52 (m, 2H, *H*-8a, *H*-5a₂), 1.49-1.44 (m, 4H, *H*-6, *H*-14), 1.33-1.30 (m, 1H, *H*-5a), 1.07 (d, 3H, *J* = 7.2 Hz, *H*-16), 1.02-0.98 (m, 4H, *H*-7a₂, *H*-15); ¹³C NMR (100 MHz, CDCl₃) δ_C 171.34 (CO), 137.61 (C-1'), 136.03 (C-6'), 132.36 (C-2'), 129.97 (C-3'), 129.13 (C-5'), 128.53 (C-4'), 104.42 (C-3), 89.96 (C-10), 88.42 (C-12), 81.01 (C-12a), 52.61 (C-5a), 45.11 (C-8a), 37.27 (C-6), 36.35 (C-4), 34.40 (C-7), 32.71 (C-9), 26.03 (C-14), 24.61 (C-5), 24.37 (C-8), 20.34 (C-15), 14.93 (C-16); ESI-HRMS: *m/z* Calcd for C₂₂H₂₈NaO₆S 443.1504. Found: 443.1504 [M+Na]⁺.

The title compounds **8a** and **8b** were synthesized from 4-mercaptobenzoic acid (**8**) by the general procedure described above.

10- α -S-[4'-(Carboxyphenyl)]-10-deoxoartemisinin (8a**)**

Brownish solid (yield, 60%); mp 73.5-80.2 °C; $[\alpha]_D^{24} +6.6^\circ$ (c 1.0, CH₂Cl₂); IR (Neat) ν_{\max} 2924, 2851, 1685, 1594, 1275, 1259, 1130, 1034, 924, 764, 750 cm⁻¹; ¹H NMR (400 MHz, CDCl₃) δ_H 8.01 (d, 2H, *J* = 8.4 Hz, *H*-3',5'), 7.74 (d, 2H, *J* = 8.4 Hz, *H*-2',6'), 5.40 (s, 1H, *H*-12), 4.85 (d, 1H, *J* = 11.2 Hz, *H*-10), 2.74-2.68 (m, 1H, *H*-9), 2.39 (dt, 1H, *J* = 3.9 Hz, *J* = 13.9 Hz, *J* = 14.1 Hz, *H*-4a₁), 2.08-2.02 (m, 1H, *H*-4a₂), 1.93-1.87 (m, 1H, *H*-5a₁), 1.77-1.70 (m, 2H, *H*-8a₁, *H*-7a₁), 1.63-1.58 (m, 1H, *H*-8a), 1.56-1.50 (m, 1H, *H*-5a₂), 1.47 (s, 3H, *H*-14), 1.46-1.39 (m, 2H, *H*-6, *H*-8a₂), 1.30-1.27 (m, 1H, *H*-5a), 1.08-1.01 (m, 1H, *H*-7a₂), 0.96 (d, 3H, *J* = 6.2 Hz, *H*-16), 0.90 (d, 3H, *J* = 7.1 Hz, *H*-15); ¹³C NMR (100 MHz, CDCl₃) δ_C 171.46 (CO), 141.50 (C-1'), 130.91 (C-4'), 130.36 (C-2', C-3', C-5', C-6'), 104.54 (C-3), 92.26 (C-12), 82.76 (C-10), 80.29 (C-12a), 51.72 (C-5a), 45.98 (C-8a), 37.40 (C-6), 36.21 (C-4), 33.99 (C-7), 31.01 (C-9), 25.96 (C-14), 24.75 (C-5), 21.28 (C-8), 20.22 (C-15), 15.04 (C-16); ESI-HRMS: *m/z* Calcd for C₂₂H₂₈NaO₆S 443.1504. Found: 443.1502 [M+Na]⁺.

10- β -S-[4'-(Carboxyphenyl)]-10-deoxoartemisinin (8b**) [28]**

Solid (yield, 28%); mp 106-108.7 °C; $[\alpha]_D^{24} +185.5^\circ$ (c 1.0, CHCl₃); IR (Neat) ν_{\max} 3418, 2955, 2925, 2871, 1689, 1594, 1455, 1417, 1378, 1290, 1229, 1186, 1131, 1089, 1040, 1014, 985, 932, 898, 878, 844, 765, 687, 537 cm⁻¹; ¹H NMR (400 MHz, CDCl₃) δ_H 7.99 (d, 2H, *J* = 7.8 Hz, *H*-3',5'), 7.60 (d, 2H, *J* = 7.8 Hz, *H*-2',6'), 5.76 (d, 1H, *J* = 5.2 Hz, *H*-10), 5.69 (s, 1H, *H*-12), 3.19-3.17 (m, 1H, *H*-9), 2.39 (dt, 1H, *J* = 3.0 Hz, *J* = 14.0 Hz, *J* = 14.0 Hz, *H*-4a₁), 2.06 (d, 1H, *J* = 14.4 Hz, *H*-4a₂), 1.91-1.73 (m, 4H, *H*-5a₁, *H*-8, *H*-7a₁), 1.60-1.45 (m, 6H, *H*-8a, *H*-5a₂, *H*-14, *H*-6), 1.33-1.31 (m, 1H, *H*-5a), 1.06-0.97 (m, 7H, *H*-16, *H*-7a₂, *H*-15); ¹³C NMR (100 MHz, CDCl₃) δ_C 173.98 (CO), 144.82 (C-1'), 130.54 (C-3', C-5'), 130.32 (C-4'), 128.55 (C-2', C-6'), 104.47 (C-3), 88.56 (C-10), 88.28 (C-12), 80.98 (C-12a), 52.59 (C-5a), 45.06 (C-8a), 37.28 (C-6), 36.32 (C-4), 34.37 (C-7), 32.70 (C-9), 26.05 (C-14), 24.58 (C-5), 24.36 (C-8), 20.32 (C-15), 14.81 (C-16); ESI-HRMS: *m/z* Calcd for C₂₂H₂₈NaO₆S 443.1504. Found: 443.1502 [M+Na]⁺.

The title compounds **9a** and **9ab** were synthesized from methyl 2-(4-mercaptophenyl)acetate (**9**) by the general procedure described above.

10-Deoxo-10- α -S-[4'-(methoxycarbonylmethyl)phenyl]-artemisinin (9a)

Colorless solid (yield, 58%); mp 75.6-84.3 °C; $[\alpha]_D^{24} +19.9^\circ$ (c 1.0, CH₂Cl₂); IR (Neat) ν_{\max} 3779, 2926, 1741, 1376, 1275, 1260, 1151, 1034, 927, 879, 764, 749 cm⁻¹; ¹H NMR (400 MHz, CDCl₃) δ_H 7.66 (d, 2H, $J = 8.3$ Hz, $H-2',6'$), 7.23 (d, 2H, $J = 8.3$ Hz, $H-3',5'$), 5.35 (s, 1H, $H-12$), 4.73 (d, 1H, $J = 10.8$ Hz, $H-10$), 3.71 (s, 3H, O-CH₃), 3.62 (s, 2H, $H-2''$), 2.61-2.56 (m, 1H, $H-9$), 2.39 (dt, 1H, $J = 4.0$ Hz, $J = 14.4$ Hz, $J = 13.6$ Hz, $H-4a_1$), 2.08-2.02 (m, 1H, $H-4a_2$), 1.92-1.87 (m, 1H, $H-5a_1$), 1.76-1.70 (m, 2H, $H-8a_1$, $H-7a_1$), 1.60-1.48 (m, 5H, $H-8a$, $H-5a_2$, $H-14$), 1.41-1.33 (m, 2H, $H-8a_2$, $H-6$), 1.28-1.23 (m, 1H, $H-5a$), 1.07-1.00 (m, 1H, $H-7a_2$), 0.97 (d, 3H, $J = 6.3$ Hz, $H-16$), 0.91 (d, 3H, $J = 7.1$ Hz, $H-15$); ¹³C NMR (100 MHz, CDCl₃) δ_C 171.88 (CO), 133.03 ($C-1'$) 132.68 ($C-2'$, 6'), 131.75 ($C-4'$), 129.52 ($C-3'$, 5'), 104.33 ($C-3$), 92.19 ($C-12$), 83.48 ($C-10$), 80.29 ($C-12a$), 52.10 (OCH₃), 51.74 ($C-5a$), 45.99 ($C-8a$), 40.82 ($C-2''$), 37.40 ($C-6$), 36.23 ($C-4$), 34.05 ($C-7$), 31.03 ($C-9$), 26.00 ($C-14$), 24.77 ($C-5$), 21.38 ($C-8$), 20.23 ($C-15$), 15.07 ($C-16$); ESI-HRMS: m/z Calcd for C₂₄H₃₂NaO₆S 471.1817. Found: 471.1817 [M+Na]⁺.

10-Deoxo-10- α/β -S-[4'-(methoxycarbonylmethyl)phenyl]-artemisinin (9ab)

Syrup (yield, 30%, $\alpha:\beta = 2:1$); $[\alpha]_D^{24} +107.8^\circ$ (c 1.0, CH₂Cl₂); IR (Neat) ν_{\max} 3454, 2953, 1739, 1494, 1453, 1406, 1368, 1341, 1256, 1222, 1155, 1118, 1081, 1017, 1034, 946, 926, 883, 807, 750 cm⁻¹; ¹H NMR (400 MHz, CDCl₃) δ_H 7.64 (d, 4H, $J = 8.2$ Hz, $\alpha H-2',6'$), 7.49 (d, 2H, $J = 8.2$ Hz, $\beta H-2',6'$), 7.21 (d, 6H, $J = 8.2$ Hz, $\alpha/\beta H-3',5'$), 5.72 (s, 1H, $\beta H-12$), 5.53 (d, 1H, $J = 5.6$ Hz, $\beta H-10$), 5.33 (s, 2H, $\alpha H-12$), 4.70 (d, 2H, $J = 10.8$ Hz, $\alpha H-10$), 3.69 (s, 6H, α O-CH₃), 3.68 (s, 3H, β O-CH₃), 3.60 (s, 4H, $\alpha H-2''$), 3.59 (s, 2H, $\beta H-2''$), 3.15-3.07 (m, 1H, $\beta H-9$), 2.60-2.54 (m, 2H, $\alpha H-9$), 2.40-2.32 (m, 3H, $\alpha/\beta H-4a_1$), 2.06-2.00 (m, 3H, $\alpha/\beta H-4a_2$), 1.91-1.77 (m, 5H, $\alpha/\beta H-5a_1$, $\beta H-8a_1$, $\beta H-8a_2$), 1.81-1.68 (m, 5H, $\alpha H-8a_1$, $\alpha/\beta H-7a_1$), 1.58-1.43 (m, 16H, $\alpha/\beta H-8a$, $\alpha/\beta H-5a_2$, $\alpha/\beta H-14$, $\beta H-6$), 1.39-1.27 (m, 6H, $\alpha H-8a_2$, $\alpha H-6$, $\alpha H-5a$), 1.24-1.22 (m, 1H, $\beta H-5a$), 1.05-0.94 (m, 15H, $\alpha/\beta H-7a_2$, $\alpha/\beta H-15$, $\beta H-16$), 0.88 (d, 6H, $J = 7.1$ Hz, $\alpha H-16$); ¹³C NMR (100 MHz, CDCl₃) δ_C 171.87 (α CO), 171.82 (β CO) 135.68 ($\beta C-1'$), 133.03 ($\alpha C-1'$), 132.68 ($\alpha C-2',6'$), 132.60 ($\beta C-4'$), 131.75, ($\alpha C-4'$), 131.18 ($\beta C-2'$, 6'), 129.79 ($\beta C-3'$, 5'), 129.51 ($\alpha C-3'$, 5'), 104.32 ($\alpha/\beta C-3$), 92.19 ($\alpha C-12$), 90.26 ($\beta C-10$), 88.36 ($\beta C-12$), 83.48 ($\alpha C-10$), 81.07 ($\beta C-12a$), 80.29 ($\alpha C-12a$), 52.65 ($\alpha C-5a$), 52.09 (α/β OCH₃), 51.74 ($\beta C-5a$), 45.99 ($\alpha C-8a$), 45.18 ($\beta C-8a$), 40.81 ($\alpha/\beta C-2''$), 37.40 ($\alpha C-6$), 37.27 ($\beta C-6$), 36.40 ($\beta C-4$), 36.23 ($\alpha C-4$), 34.43 ($\beta C-7$), 34.06 ($\alpha C-7$), 32.73 ($\beta C-9$), 31.03 ($\alpha C-9$), 26.10 ($\beta C-14$), 26.00 ($\alpha C-14$), 24.77 ($\alpha C-5$), 24.62 ($\beta C-5$), 24.37 ($\beta C-8$), 21.38 ($\alpha C-8$), 20.34 ($\beta C-15$), 20.23 ($\alpha C-15$), 15.07

(α C-16), 14.97 (β C-16); ESI-HRMS: m/z Calcd for $C_{24}H_{32}NaO_6S$ 471.1817 Found: 471.1813 $[M+Na]^+$.

The title compounds **10a** and **10b** were synthesized from 4-chlorothiophenol (**10**).

10- α -S-(4'-Chlorophenyl)-10-deoxyartemisinin (10a)

Colorless solid (yield, 66%); mp 139.8-142.9 °C; $[\alpha]_D^{24}$ +87.4° (c 1.0, CH_2Cl_2); IR (Neat) ν_{max} 2926, 2862, 1475, 1377, 1195, 1128, 1093, 1035, 1013, 927, 879, 826 cm^{-1} ; 1H NMR (400 MHz, $CDCl_3$) δ_H 7.64 (d, 2H, $J = 8.6$ Hz, $H-2',6'$), 7.26 (d, 2H, $J = 8.6$ Hz, $H-3',5'$), 5.34 (s, 1H, $H-12$), 4.68 (d, 1H, $J = 10.8$ Hz, $H-10$), 2.56-2.50 (m, 1H, $H-9$), 2.36 (dt, 1H, $J = 4.0$ Hz, $J = 14.5$ Hz, $J = 13.5$ Hz, $H-4a_1$), 2.06-2.00 (m, 1H, $H-4a_2$), 1.91-1.84 (m, 1H, $H-5a_1$), 1.75-1.69 (m, 2H, $H-8a_1$, $H-7a_1$), 1.54-1.51 (m, 1H, $H-8a$), 1.50-1.41 (m, 4H, $H-5a_2$, $H-14$), 1.39-1.29 (m, 2H, $H-8a_2$, $H-6$), 1.27-1.19 (m, 1H, $H-5a$), 1.06-0.99 (m, 1H, $H-7a_2$), 0.95 (d, 3H, $J = 6.3$ Hz, $H-16$), 0.87 (d, 3H, $J = 7.1$ Hz, $H-15$); ^{13}C NMR (100 MHz, $CDCl_3$) δ_C 134.07 (C-2', 6'), 133.55 (C-1'), 131.00, (C-4') 128.73 (C-3', 5'), 104.36 (C-3), 92.21 (C-12), 83.24 (C-10), 80.25 (C-12a), 51.67 (C-5a), 45.90 (C-8a), 37.40 (C-6), 36.18 (C-4), 34.02 (C-7), 30.83 (C-9), 25.97 (C-14), 24.75 (C-5), 21.37 (C-8), 20.20 (C-15), 14.93 (C-16); ESI-HRMS: m/z Calcd for $C_{21}H_{27}ClNaO_4S$ 433.1216. Found: 433.1216 $[M+Na]^+$.

10- β -S-(4'-Chlorophenyl)-10-deoxyartemisinin (10b)

Colorless solid (yield, 26%); mp 68.6-69.8 °C; $[\alpha]_D^{24}$ +301.4° (c 1.0, CH_2Cl_2); IR (Neat) ν_{max} 2926, 2862, 1475, 1377, 1195, 1128, 1093, 1035, 1013, 927, 879, 826 cm^{-1} ; 1H NMR (400 MHz, $CDCl_3$) δ_H 7.47 (d, 2H, $J = 8.6$ Hz, $H-2',6'$), 7.25 (d, 2H, $J = 8.6$ Hz, $H-3',5'$), 5.71 (s, 1H, $H-12$), 5.51 (d, 1H, $J = 5.3$ Hz, $H-10$), 3.14-3.10 (m, 1H, $H-9$), 2.38 (dt, 1H, $J = 3.9$ Hz, $J = 13.9$ Hz, $J = 14.2$ Hz, $H-4a_1$), 2.07-2.02 (m, 1H, $H-4a_2$), 1.91-1.87 (m, 1H, $H-5a_1$), 1.81-1.70 (m, 3H, $H-8$, $H-7a_1$), 1.58-1.50 (m, 3H, $H-8a$, $H-5a_2$, $H-6$), 1.43 (s, 3H, $H-14$), 1.32-1.26 (m, 2H, $H-5a$, $H-7a_2$), 1.04 (d, 3H, $J = 7.3$ Hz, $H-16$), 0.97 (d, 3H, $J = 6.3$ Hz, $H-15$); ^{13}C NMR (100 MHz, $CDCl_3$) δ_C 135.35 (C-1'), 132.92 (C-4'), 132.28 (C-2', 6'), 128.96 (C-3', 5'), 104.34 (C-3), 90.34 (C-12), 88.36 (C-10), 80.99 (C-12a), 52.61 (C-5a), 45.10 (C-8a), 37.27 (C-6), 36.36 (C-4), 34.39 (C-7), 32.71 (C-9), 26.06 (C-14), 24.60 (C-5), 24.34 (C-8), 20.31 (C-15), 14.89 (C-16); ESI-HRMS: m/z Calcd for $C_{21}H_{27}ClNaO_4S$ 433.1216. Found: 433.1216 $[M+Na]^+$.

The title compound **11a** was synthesized from 4-nitrothiophenol (**11**).

10-Deoxo-10- α -S-(4'-nitrophenyl)-artemisinin (11a)

Colorless solid (yield, 78%); mp 133.3-139.5 °C; $[\alpha]_D^{24}$ +36.5° (c 0.5, CH₂Cl₂); IR (Neat) ν_{\max} 2926, 2869, 1579, 1514, 1338, 1093, 1035, 1004, 933, 852, 742 cm⁻¹; ¹H NMR (400 MHz, CDCl₃) δ_H 8.13 (d, 2H, J = 8.9 Hz, H -3', H -5'), 7.83 (d, 2H, J = 8.9 Hz, H -2', H -6'), 5.41 (s, 1H, H -12), 4.86 (d, 1H, J = 10.9 Hz, H -10), 2.75-2.69 (m, 1H, H -9), 2.39 (dt, 1H, J = 3.8 Hz, J = 14.3 Hz, J = 13.9 Hz, H -4a₁), 2.09-2.03 (m, 1H, H -4a₂), 1.95-1.88 (m, 1H, H -5a₁), 1.77-1.71 (m, 2H, H -8a₁, H -7a₁), 1.64-1.60 (m, 1H, H -8a), 1.51-1.39 (m, 6H, H -5a₂, H -14, H -8a₂, H -6), 1.33-1.28 (m, 1H, H -5a), 1.10-1.02 (m, 1H, H -7a₂), 0.97 (d, 3H, J = 6.2 Hz, H -16), 0.89 (d, 3H, J = 7.1 Hz, H -15); ¹³C NMR (100 MHz, CDCl₃) δ_C 146.28 (C -4'), 143.46 (C -1'), 130.65 (C -2', C -6'), 123.63 (C -3', C -5'), 104.60 (C -3), 92.31 (C -12), 82.55 (C -10), 80.28 (C -12a), 51.65 (C -5a), 45.88 (C -8a), 37.41 (C -6), 36.14 (C -4), 33.93 (C -7), 30.81 (C -9), 25.95 (C -14), 24.71 (C -5), 21.23 (C -8), 20.19 (C -15), 14.96 (C -16); ESI-HRMS: m/z Calcd for C₂₁H₂₇NNaO₆S 444.1457. Found: 444.1456 [M+Na]⁺.

The title compounds **12a** and **12b** were synthesized from 2-quinolinethiol (**12**).

10-Deoxo-10- α -S-(2'-quinolino)-artemisinin (12a)

Pale yellow solid (yield, 52%); mp 116.3-120.7 °C; $[\alpha]_D^{24}$ -107.22° (c 1.0, CH₂Cl₂); IR (Neat) ν_{\max} 2926, 1591, 1454, 1374, 1288, 1194, 1122, 1085, 1034, 926, 876, 822 cm⁻¹; ¹H NMR (400 MHz, CDCl₃) δ_H 7.94 (d, 2H, J = 8.5 Hz, H -3', 4'), 7.72 (d, 1H, J = 8.1 Hz, H -5'), 7.64 (t, 1H, J = 7.0 Hz, H -6'), 7.49 (d, 1H, J = 8.6 Hz, H -8'), 7.43 (t, 1H, J = 6.9 Hz, H -7'), 5.95 (d, 1H, J = 11.2 Hz, H -10), 5.49 (s, 1H, H -12), 2.86-2.80 (m, 1H, H -9), 2.39 (dt, 1H, J = 4.0 Hz, J = 13.7 Hz, J = 13.4 Hz, H -4a₁), 2.06-2.01 (m, 1H, H -4a₂), 1.93-1.87 (m, 1H, H -5a₁), 1.86-1.77 (m, 2H, H -8a₁, H -7a₁), 1.72-1.61 (m, 2H, H -8a, H -5a₂), 1.54-1.43 (m, 5H, H -14, H -8a₂, H -6), 1.34-1.26 (m, 1H, H -5a), 1.10-1.04 (m, 1H, H -7a₂), 1.01-0.99 (m, 6H, H -16, H -15); ¹³C NMR (100 MHz, CDCl₃) δ_C 131.50, 127.89, 104.13, 96.42, 94.63, 91.21, 87.80, 81.13, 80.36, 52.50, 51.53, 45.44, 44.31, 37.48, 36.37, 34.79, 30.78, 26.08, 25.98, 24.71, 22.13, 20.38, 13.19, 12.72; ESI-HRMS: m/z Calcd for C₂₄H₂₉NNaO₄S 450.1715. Found: 450.1718 [M+Na]⁺.

10-Deoxo-10- β -S-(2'-quinolino)-artemisinin (12b)

Pale yellow solid (yield, 39%); mp 102.7-113.5 °C; $[\alpha]_D^{24} +61.4^\circ$ (c 1.0, CH₂Cl₂); IR (Neat) ν_{\max} 3413, 2926, 1725, 1591, 1454, 1374, 1288, 1194, 1122, 1085, 1034, 926, 876, 822 cm⁻¹; ¹H NMR (400 MHz, CDCl₃) δ_H 7.97 (d, 1H, *J* = 8.5 Hz, *H*-3'), 7.93 (d, 1H, *J* = 8.7 Hz, *H*-4'), 7.70 (d, 1H, *J* = 8.0 Hz, *H*-5'), 7.64 (t, 1H, *J* = 8.4 Hz, *H*-6'), 7.42 (t, 1H, *J* = 8.0 Hz, *H*-7'), 7.36 (d, 1H, *J* = 8.6 Hz, *H*-8'), 6.93 (d, 1H, *J* = 5.3 Hz, *H*-10), 5.63 (s, 1H, *H*-12), 3.34-3.26 (m, 1H, *H*-9), 2.39 (dt, 1H, *J* = 3.9 Hz, *J* = 14.3 Hz, *J* = 13.6 Hz, *H*-4a₁), 2.06-2.01 (m, 1H, *H*-4a₂), 1.92-1.70 (m, 4H, *H*-5a₁, *H*-8, *H*-7a₁), 1.64-1.59 (m, 1H, *H*-8a), 1.57-1.49 (m, 1H, *H*-5a₂), 1.47-1.38 (m, 4H, *H*-6, *H*-14), 1.34-1.26 (m, 1H, *H*-5a), 1.06 (d, 3H, *J* = 7.3 Hz, *H*-16), 1.03-1.00 (m, 1H, *H*-7a₂), 0.98 (d, 3H, *J* = 6.3 Hz, *H*-15); ¹³C NMR (100 MHz, CDCl₃) δ_C 157.96 (*C*-2'), 148.07 (*C*-8a'), 136.08 (*C*-4'), 129.68 (*C*-7'), 128.47 (*C*-8'), 127.44 (*C*-5'), 126.38 (*C*-6'), 125.54 (*C*-4a'), 121.45 (*C*-3'), 104.36 (*C*-3), 89.16 (*C*-12), 84.03 (*C*-10), 80.99 (*C*-12a), 52.66 (*C*-5a), 45.24 (*C*-8a), 37.33 (*C*-6), 36.32 (*C*-4), 34.46 (*C*-7), 32.17 (*C*-9), 26.06 (*C*-14), 24.60 (*C*-5), 24.16 (*C*-8), 20.32 (*C*-15), 14.73 (*C*-16); ESI-HRMS: *m/z* Calcd for C₂₄H₂₉NNaO₄S 450.1715. Found: 450.1717 [M+Na]⁺.

The title compounds **13a** and **13b** were synthesized from 5-mercapto-1-methyltetrazole (**13**).

10-Deoxo-10-β-S-[5'-(1'-methyltetrazolo)]-artemisinin (**13a**)

Colorless solid (yield, 69%); mp 53.4-68.8 °C; $[\alpha]_D^{24} +7.4^\circ$ (c 1.0, CH₂Cl₂); IR (Neat) ν_{\max} 2926, 2876, 1456, 1411, 1354, 1309, 1266, 1197, 1125, 1090, 1039, 1015, 928, 879, 822 cm⁻¹; ¹H NMR (400 MHz, CDCl₃) δ_H 6.72 (d, 1H, *J* = 10.4 Hz, *H*-10), 5.56 (s, 1H, *H*-12), 3.90 (s, 3H, N-CH₃), 2.54-2.49 (m, 1H, *H*-9), 2.39-2.32 m, 1H, *H*-4a₁), 2.08-2.03 (m, 1H, *H*-4a₂), 1.98-1.94 (m, 1H, *H*-5a₁), 1.88-1.84 (m, 1H, *H*-8a₁), 1.68-1.64 (m, 1H, *H*-7a₁), 1.61-1.52 (m, 3H, *H*-8a, *H*-5a₂, *H*-6), 1.50 (s, 3H, *H*-14), 1.45-1.38 (m, 1H, *H*-8a₂), 1.37-1.32 (m, 1H, *H*-5a), 1.09-1.02 (m, 4H, *H*-7a₂, *H*-16), 0.98 (d, 3H, *J* = 6.0 Hz, *H*-15); ¹³C NMR (100 MHz, CDCl₃) δ_C 166.03 (*C*-5'), 102.82 (*C*-3), 90.95 (*C*-12), 83.37 (*C*-10), 82.06 (*C*-12a), 51.00 (*C*-5a), 47.27 (*C*-8a), 38.63 (*C*-6), 37.19 (*C*-4), 36.15 (*C*-7), 34.43 (NCH₃), 33.94 (*C*-9), 31.56 (*C*-14), 25.60 (*C*-5), 24.69 (*C*-8), 19.77 (*C*-15), 18.04 (*C*-16); ESI-HRMS: *m/z* Calcd for C₁₇H₂₆N₄NaO₄S 405.1572. Found: 405.1572 [M+Na]⁺.

10-Deoxo-10-β-S-[5'-(1'-methyltetrazolo)]-artemisinin (**13b**)

Colorless solid (yield, 22%); mp 154.6-159.3 °C; $[\alpha]_D^{24} +41.9^\circ$ (c 1.0, CH₂Cl₂); IR (Neat) ν_{\max} 3427, 2926, 2876, 1736, 1613, 1456, 1411, 1354, 1309, 1266, 1197, 1125, 1090, 1039, 1015, 928, 879, 822 cm⁻¹; ¹H NMR (400 MHz, CDCl₃) δ_H 6.62 (d, 1H, *J* = 6.3 Hz, *H*-10), 6.05 (s, 1H, *H*-12), 3.88 (s, 3H, N-CH₃), 3.28-3.26 (m, 1H, *H*-9), 2.40 (dt, 1H, *J* = 4.01 Hz, *J* = 14.6 Hz, *J* = 13.4 Hz, *H*-4a₁), 2.09-2.04 (m, 1H, *H*-4a₂), 1.95-1.90 (m, 2H, *H*-5a₁), 1.72-1.61 (m, 3H, *H*-8, *H*-7a₂), 1.55-1.45 (m, 2H, *H*-8a, *H*-5a₂), 1.43 (s, 3H, *H*-14), 1.38-1.34 (m, 1H, *H*-6), 1.32-1.28 (m, 1H, *H*-5a), 1.00-0.94 (m, 4H, *H*-16, *H*-7a₂), 0.90 (d, 3H, *J* = 7.4 Hz, *H*-15); ¹³C NMR (100 MHz, CDCl₃) δ_C 165.72 (*C*-5'), 104.41 (*C*-3), 90.87 (*C*-12), 86.12 (*C*-10), 80.41 (*C*-12a), 52.46 (*C*-5a), 43.68 (*C*-8a), 37.09 (*C*-6), 36.13 (*C*-4), 34.56 (*C*-7), 34.32 (NCH₃), 30.59 (*C*-9), 25.80 (*C*-14), 24.56 (*C*-5), 22.58 (*C*-8), 20.19 (*C*-15), 12.61 (*C*-16); ESI-HRMS: *m/z* Calcd for C₁₇H₂₆N₄NaO₄S 405.1572. Found: 405.1572 [M+Na]⁺.

Biological methods

Cell lines and reagents

Human prostate carcinoma PC-3 cells and other cell lines were purchased from National Center for Cell Science, Pune, India) and were cultured in RPMI-1640 and DMEM media, purchased from Invitrogen (California, USA) supplemented with 10,000 units/mL, penicillin and 10 mg/mL streptomycin in 0.9% normal saline, purchased from HIMEDIA and 10% heat-inactivated fetal calf serum purchased from Invitrogen (California, USA). Cell culture grade DMSO, MTT reagent, artemisinin and MG-132 were purchased from Sigma Aldrich (USA). *N*-Acetyl-L-cysteine, crystal violet, and doxorubicin were purchased from HIMEDIA (Vadhani Ind., East Mumbai). Propidium iodide was purchased from BD Biosciences (USA). The antibodies against E2F1, Pin1, Bcl-xL, procaspase-3, eIF4E and c-Myc were purchased from Santa Cruz Biotechnology (Dallas, Texas, USA). The anti-procaspase-9, PCNA and Cyclin D1 antibodies were purchased from Cloud-Clone Corp (Texas, USA). The anti-c-jun and phospho-c-jun antibodies were purchased from Abcam (Cambridge, UK) and cell signaling (Danvers, USA) respectively. Mouse monoclonal IgG1 β -actin, goat anti-rabbit IgG- HRP and goat anti-mouse IgG were obtained from Sigma Life Science (USA). Bio-Rad Clarity™ Western ECL substrate, SYBR-iTAQ Universal SYBR Green super mix were purchased from Bio-Rad Laboratories (California, USA). siRNAs were obtained from Qiagen, (Hilden, Germany). Hoechst 33342 CM-

H2DCFDA, TRIzol, Lipofectamine RNAiMAX and Opti-MEM were purchased from Invitrogen (California, USA).

Cell culture and treatment

PC-3 cells were cultured in RPMI-1640 medium supplemented with 10% fetal bovine serum and penicillin-streptomycin at 37 °C in 5% CO₂ incubator. Cells were treated with varying concentrations of **9a** (0.1, 0.3, 1, 3 and 10 μM) dissolved in DMSO for 72 h. The percentage of DMSO was 0.1% in each treatment. Doxorubicin was used as positive control in MTT experiments. 0.1% DMSO was used as vehicle control.

MTT assay (cell viability assay)

The colorimetric MTT (3-(4,5-dimethylthiazol-2-yl)-2,5-diphenyltetrazolium bromide) assay was used to measure the cell viability of different cells following treatment with *S*-linked artemisinin derivatives. Briefly cells were seeded in a 96 well plate at a density of 3000 cells/well. Following attachment the cells were treated with varying concentrations (0.1-10 μM) of **9a** in media and were kept for incubation for 72 h. MTT (20 μL, 5 mg/mL in PBS) was added to each well and the cells were incubated for another 3 h at 37 °C. The supernatant was removed carefully and 150 μL of DMSO was added to each well to dissolve the MTT formazan crystals. The plate was shaken on a rocker for 15-20 min and the absorbance values of samples in each of the wells were determined using a multi-well plate reader (Biotek, Winooski, USA) at 570 nm. The wells treated with DMSO and doxorubicins were taken as the vehicle control and the positive control, respectively. Data were also obtained similarly for all the replicates and the percentage viability was determined with respect to the DMSO-treated cells.

Colony formation assay

The PC-3 cells were seeded in six-well plate at a density of 500 cells per well. Following adherence of the cells (left for overnight), the cells were treated with **9a**. After every 72 h, the media was changed and the cells were treated with **9a** and the experiments lasted for 15 days. After the colony development, the wells were washed with PBS, fixed with 3.7% formaldehyde for 20 min, washed with PBS and then were stained using 0.4% crystal violet followed by rinsing the wells with PBS four to five times. The colonies were counted using Image J software. Similar experiments were also carried out with artemisinin in order to facilitate a comparison of the results with those obtained using **9a**.

ROS scavenging experiment

Briefly, the PC-3 cells cultured on the 96-well plate were pre-treated with ROS scavenger, *N*-acetyl cysteine (NAC 20 μ M) for 2 h followed by treatment of the cells with **9a** (3 and 10 μ M). The viability of the cells in the presence of NAC treated with **9a** was assayed by MTT assay as explained above.

Measurement of the intracellular ROS levels

The level of ROS in the PC-3 cells following treatment with **9a** was measured using the fluoroprobe, CM-H2DCFDA. Approximately 1×10^5 cells were cultured in each well of the six-well plate and treated with the 3 μ M and 10 μ M of **9a** for 3 h. The media was removed and the cells were incubated with 10 μ M CM-H2DCFDA in fresh media for 30 min in the dark at 37 °C. The cells were then stained with Hoechst 33342 (1 μ g/mL) for nuclear staining, kept in the dark for 15 min at room temperature followed by washing of the wells with PBS. Images were captured using a fluorescence microscope (Nikon Ti).

JC-1 Staining

PC-3 cells treated with 3 and 10 μ M of **9a** and artemisinin, separately, for 48 h were stained with cationic dye JC-1 (10 μ M) and kept in dark for 30 min to analyze the mitochondrial membrane potential by fluorescence microscope.

Cell cycle analysis

1.5×10^5 PC-3 cells/well were seeded into 6 well plates and left for adherence. Following the attachment of the cells, treatment with 3 and 10 μ M of **9a** and artemisinin, separately, was given and were incubated for 48 h. After this the cells were harvested and fixed with ice cold 80% ethanol and kept overnight at 4°C. Next, the cells were washed with PBS to remove ethanol, and centrifuged at 1800 rpm for 5 minutes, after which cells were treated with RNase (50 U/mL) and propidium iodide (20 μ g/mL) for 30 min at room temperature and further subjected to flow cytometry (BD FACS Verse™) to analyze DNA content. Samples were run at low speed and a minimum of 50,000 events were recorded and analyzed by ModFit LT software (Verity Software House, USA).

Apoptosis and cell death assays

The changes in the cellular morphology, Hoechst 33342 staining, and the flow cytometry experiments were done to evaluate apoptosis. The PC-3 cells treated with 3 μ M and 10 μ M of **9a**

for 72 h were observed by a microscope (Nikon Ti) for apoptotic morphology. For Hoechst 33342 staining, the cells treated with 3 μ M and 10 μ M of **9a** and artemisinin, separately, for 72 h were stained with Hoechst 33342 stain for 15 min at room temperature in the dark. The cells were then washed with PBS once and were visualized under a Nikon fluorescent microscope. For the flow cytometry study, the PC-3 cells were cultured in a six-well culture plate, incubated with concentrations 3 μ M and 10 μ M of **9a** for 72 h. The cells were harvested, washed with PBS and were then incubated with propidium iodide (5 μ g/mL) for 20 min at 4 °C. The samples were acquired using FACS verse (BD Biosciences) for cell death using flow cytometry. The cells with DMSO treatment were taken as the control.

Wound healing assay

PC-3 cells (3×10^5) were seeded to each well of 6 well plates and cultured at 37 °C in 5% CO₂ until mono-layer was formed. The scratch at 90 degree was generated by using a 200 μ L pipette tip. After this the mono-layer was washed to remove the detached cells and treated with **9a** and artemisinin, separately (3 μ M and 10 μ M). The images were captured at 0 h and up to 8 h at 2 h interval each.

Transwell Assay

The migration assay was performed using Transwell permeable supports (6.5mm insert and 8.0 μ m polycarbonate membrane, Corning). The lower chamber was supplemented with RPMI-1640 containing 10%FBS whereas upper chamber consisted of serum free media with 40,000 cells in each chamber of control and treatments (3 μ M and 10 μ M of **9a**). Following the treatment period of 48 h the media was removed and the upper chambers were cleaned with cotton swab for non-migrating cells. Whereas, the migrating cells were fixed in 75% ethanol for 10 min and later stained with Hoechst stain.

Gelatin zymography

PC-3 cells were cultured in a 6 well plate and were allowed to form mono layer following which an injury line was made with 200 μ L pipette and then treated with **9a** (3 μ M and 10 μ M) in serum containing media for 48 h and then washed with serum-free media and further kept for 24 h in serum-free media. The collected serum-free media was mixed with 5X non-reducing sample buffer (4% SDS, 20% glycerol, 0.01% bromophenol blue, 125 mM Tris-HCl, pH 6.8) and was

subjected to electrophoresis on 7.5% SDS-PAGE containing 4mg/mL gelatin. After washing with the washing buffer for 30 min (2.5% Triton X-100, 50 mM Tris HCl, pH, 7.5, 5 mM CaCl₂, 1 μM ZnCl₂) the gel was incubated in the incubation buffer (1% Triton X-100, 50 mM Tris HCl, pH 7.5, 5 mM CaCl₂, 1 μM ZnCl₂) at 37 °C for 24 h. On the next day the gel was stained with staining solution (40% methanol, 10% acetic acid, 0.5% coomassie blue) and was destained with the destaining solution (40% methanol and 10% acetic acid, v/v solution). The gelatinolytic activity was detected as clear band against blue background.

Western Blotting

The PC-3 cells (1.25×10^5) were seeded into each well of six-well plates and were exposed to different concentrations of **9a** (0.1, 0.3, 1, 3, and 10 μM) for 72 h. Following incubation, the cells were washed with cold PBS and lysed using 2XSDS lysis buffer (0.5 M Tris-HCl, pH 6.8, glycerol, 10%, w/v, SDS). The lysates were sonicated once for 10 sec at 30% amplitude. The protein estimation was done by BCA method and 20-25 μg protein samples were resolved on 12% polyacrylamide SDS gel and electrophoretically transferred to PVDF membranes. The membranes were then blocked with 5% BSA in TBST buffer for 1 h at room temperature, incubated with primary antibodies (1:500 and 1:1000) for overnight, and subsequently with the conjugated secondary antibody (1:5000) for 1 h at room temperature. The proteins were detected by the enhanced chemiluminescence (Bio-Rad).

Real-time PCR

The PC-3 cells (1.25×10^5 , in each well) cultured in a six-well plate were treated with 3 μM and 10 μM of **9a** for 72 h. Following incubation, the cells were washed with cold PBS and were then incubated with the TRIZOL reagent to extract total RNA. cDNA was synthesized using 2 μg total RNA with a cDNA synthesis kit (Thermo). The primers of GAPDH, p21, Noxa, Bcl-xL, E2F1, PCNA and Cyclin B1 are shown in Table 5. The mRNA levels of the tabulated genes were calculated using the $2^{-\Delta\Delta C_t}$ method. 10 μL of reaction volume was used for the amplification consisting of 2.5 μL of five-fold diluted cDNA, 5 μL SYBR, 0.2 μL of each primer and sterile distilled water. Cycling condition was as follows: 10 min at 95 °C and 40 cycles of 15 sec at 95 °C, 30 sec at 60 °C and the melt curve with single reaction cycle with the following conditions: 95 °C for 15 sec, 60 °C for 1 min and dissociation at 95 °C for 15 sec. After the amplification, the cycle threshold (Ct) values were obtained and normalized to the value of housekeeping gene

GAPDH. The relative expressions of the tabulated genes were calculated using the $2^{-\Delta\Delta C_t}$ method. Experiments were repeated at least three times in triplicates (Table 6).

Table 6. List of primers and product sizes for Real-Time PCR

Genes	Forward primer(5'→3')	Reverse primer(5'→3')	Product size
p21	CTGCCCAAGCTCTACCTTCC	CGAGGCACAAGGGTACAAGA	149
Noxa	AAGAACGCTCAACCGAGCC	CTGCCGGAAGTTCAGTTTGTC	99
E2F1	ACTCAGCCTGGAGCAAGAAC	GGTGGGGAAAGGCTGATGAA	165
PCNA	TCTGAGGGCTTCGACACCTA	CATTGCCGGCGCATTTTAGT	94
Cyclin B1	AGGCGAAGATCAACATGGCA	AGCTGTTCTTGGCCTCAGTC	86
GAPDH	GTCAAGGCTGAGAACGGGAA	AAATGAGCCCCAGCCTTCTC	158
Bcl-xL	GCCCCAGAAGGGACTGAATC	AGTGGCTCCATTACCCGC	99

siRNA Transfection

To further validate Pin1 as one of the targets of **9a**, we used siRNA-mediated knockdown of Pin1 alone and in the presence of **9a** and evaluated the expression of Pin1 by western blotting. The PC-3 cells (1.5×10^5) cultured in a six-well plate were transfected with 25 nM of each siRNA diluted in Opti-Mem media. Likewise, a complex of Lipofectamine-RNAiMAX (4 μ L/well) and Opti-Mem was prepared and incubated for 5 min at room temperature. Post 5 min incubation, both of the complexes were mixed in 1:1 ratio and were incubated for 25 min at room temperature. The cells were then transfected with Opti-Mem- siRNA-Lipofectamine complex and incubated for 72 h. The sequence used in siRNA and the target sequence are mentioned below in Table 7.

Table 7. List of the sequences used in siRNA and the target sequence of mRNA

siRNA	Scramble	Pin1
Target sequence	5'-AATTCTCCGAACGTGTCACGT-3'	5'-GACCGCCAGATTCTCCTTAA-3'

Sense strand	5'-UUCUCCGAACGUGUCACGUdTdT-3'	5'-CCGCCAGAUUCUCCCUUAATT-3'
Anti-sense strand	5'-ACGUGACACGUUCGGAGAAdTdT-3'	5'-UUAAGGGAGAAUCUGGCGGTC-3'

Statistical analysis:

The results are expressed as the mean \pm standard deviation (SD). A Paired t-test was used to determine the significant difference between groups. A p-value < 0.05 was considered as significant.

Acknowledgement:

Rajesh Gour and Santosh Kumar Prajapati thank NIPER for doctoral and M.S. degree, respectively, Research Fellowships; Faiz Ahmad and Shibendra Kumar Lal Karna thank ICMR (No.3/1/3/JRF-2015) and SAU, respectively, for doctoral Research Fellowship each.

Conflict of Interest:

The authors have no conflict of interest to declare.

Abbreviations:

Bcl-xL	B-cell lymphoma-extra large
CM-H2DCFDA	5-(and-6)-Chloromethyl-2',7'-dichlorodihydrofluorescein diacetate
NAC	<i>N</i> -Acetyl-L-cysteine
Pin1	Protein never in mitosis gene A interacting 1
PCNA	Proliferating cell nuclear antigen
siRNA	Short interfering RNA

5. REFERENCES

- [1] T. K. Mutabingwa, Artemisinin-based combination therapies (ACTs): best hope for malaria treatment but inaccessible to the needy, *Acta Trop.* 95 (2005), 305-315.

- [2] S. Krishna, L. Bustamante, R. K. Haynes, H. M. Staines, Artemisinin: their growing importance in medicine, *Trends Pharmacol. Sci.* 29 (2008) 520-527.
- [3] H. J. Woerdenbag, T. A. Moskal, N. Pras, T. M. Malingre, F. S. El-Feraly, H. H. Kampinga, A. W. Konings, Cytotoxicity of artemisinin-related endoperoxides to Ehrlich ascites tumor cells, *J. Nat. Prod.* 56 (1993) 849-856.
- [4] A. Bhaw-Luximon, D. Jhurry, Artemisinin, and its derivatives in cancer therapy: status of progress, mechanism of action, and future perspectives, *Cancer Chemother. Pharmacol.* 79 (2017) 451-466.
- [5] K. Q. Tran, A. S. Tin, G. L. Firestone, Artemisinin triggers a G1 cell cycle arrest of human Ishikawa endometrial cancer cells and inhibits cyclin-dependent kinase-4 promoter activity and expression by disrupting nuclear factor- κ B transcriptional signaling, *Anticancer Drugs* 25 (2014) 270-281.
- [6] A. Hamacher-Brady, H. A. Stein, S. Turschner, I. Toegel, R. Mora, N. Jennewein, T. Efferth, R. Eils, N. R. Brady, Artesunate activates mitochondrial apoptosis in breast cancer cells via iron-catalyzed lysosomal reactive oxygen species production, *J. Biol. Chem.* 286 (2011) 6587-6601.
- [7] R. Kong, G. Jia, Z. X. Cheng, Y. W. Wang, M. Mu, S. J. Wang, S. H. Pan, Y. Gao, H. C. Jiang, D. L. Dong, B. Sun, Dihydroartemisinin enhances Apo2l/TRAIL-mediated apoptosis in pancreatic cancer cells via ROS-mediated up-regulation of death receptor 5, *PLoS One* 7 (2012) e37222.
- [8] J. J. Lu, L. H. Meng, Y. J. Cai, Q. Chen, L. J. Tong, L. P. Lin, J. Ding, Dihydroartemisinin induces apoptosis in HL-60 leukemia cells dependent on iron and p38 mitogen-activated protein kinase activation but independent of reactive oxygen species, *Cancer Biol. Ther.* 7 (2008) 1017-1023.
- [9] G. Qin, L. Wu, H. Liu, Y. Pang, C. Zhao, S. Wu, X. Wang, T. Chen, Artesunate induces apoptosis via a ROS-independent and Bax-mediated intrinsic pathway in Hep G2 cells, *Exp. Cell Res.* 336 (2015) 308-317.
- [10] S. Zhu, W. Liu, X. Ke, J. Li, R. Hu, H. Cui, G. Song, Artemisinin reduces cell proliferation and induces apoptosis in neuroblastoma, *Oncol. Rep.* 32 (2014) 1094-1100.

- [11] S. A. K. Rasheed, T. Efferth, I. A. Asangani, H. Allgayer, First evidence that the antimalarial drug artesunate inhibits invasion and in vivo metastasis in lung cancer by targeting essential extracellular proteases, *Int. J. Cancer* 127 (2010) 1475-1485.
- [12] R. Handrick, T. Ontikatze, K. D. Bauer, F. Freier, A. Rubel, J. Durig, C. Belka, V. Jendrossek, Dihydroartemisinin induces apoptosis by a Bak-dependent intrinsic pathway, *Mol. Cancer Ther.* 9 (2010) 2497-2510.
- [13] Y. Pang, G. Qin, L. Wu, X. Wang, T. Chen, Artesunate induces ROS-dependent apoptosis via a Bax-mediated intrinsic pathway in Huh-7 and Hep3B cells, *Exp. Cell Res.* 347 (2016) 251-260.
- [14] J. L. Li, W. Zhao, C. Zhou, Y. X. Zhang, H. M. Li, Y. L. Tang, X. H. Liang, T. Chen, Y. J. Tang, Comparison of carbon-sulfur and carbon-amine bond in therapeutic drug: 4 β -S-aromatic heterocyclic podophyllum derivatives display antitumor activity, *Sci. Rep.* 5 (2015) 14814-14831.
- [15] L. Pastorino, A. Sun, P. J. Lu, X. Z. Zhou, M. Balastik, G. Finn, G. Wulf, J. Lim, S. H. Li, X. Li, W. Xia, L. K. Nicholson, K. P. Lu, The prolyl isomerase Pin1 regulates amyloid precursor protein processing and amyloid- β production, *Nature* 440 (2006) 528-534.
- [16] K. Nakamura, A. Greenwood, L. Binder, E. H. Bigio, S. Denial, L. Nicholson, X. Z. Zhou, K. P. Lu, Proline isomer-specific antibodies reveal the early pathogenic tau conformation in Alzheimer's disease, *Cell* 149 (2012) 232-244.
- [17] Z. Lu, T. Hunter, Prolyl isomerase Pin1 in cancer, *Cell Res.* 24 (2014) 1033-1049.
- [18] M. Xu, C. C. M. Cheung, C. Chow, S. W. M. Lun, S. T. Cheung, K. W. Lo, Overexpression of PIN1 enhances cancer growth and aggressiveness with cyclin D1 induction in EBV-associated nasopharyngeal carcinoma, *PloS One* 11 (2016) e0156833.
- [19] G. Ayala, D. Wang, G. Wulf, A. Frolov, R. Li, J. Sowadski, T. M. Wheeler, K. P. Lu, L. Bao, The prolyl isomerase Pin1 is a novel prognostic marker in human prostate cancer, *Cancer Res.* 63 (2003) 6244-6251.
- [20] J. Fishwick, G. Edwards, S. A. Ward, W. G. McLean, Morphological and immunocytochemical effects of dihydroartemisinin on differentiating NB2a neuroblastoma cells, *Neurotoxicology*, 19 (1998) 393-403.

- [21] D. L. Wesche, M. A. DeCoster, F. C. Tortella, T. G. Brewer, Neurotoxicity of artemisinin analogs in vitro, *Antimicrob. Agents Chemother.* 38 (1994) 1813-1819.
- [22] Q. G. Li, J. O. Peggins, L. L. Fleckenstein, K. Masonic, M. H. Heiffer, T. G. Brewer, The pharmacokinetics and bioavailability of dihydroartemisinin, arteether, artemether, artesunic acid and artelinic acid in rats, *J. Pharm. Pharmacol.* 50 (1998) 173-182.
- [23] P. M. O'Neill, M. Pugh, A. V. Stachulski, S. A. Ward, J. Davies, B. K. Park, Optimisation of the allylsilane approach to C-10 deoxy carba analogs of dihydroartemisinin: synthesis and in vitro antimalarial activity of new, metabolically stable C-10 analogs, *J. Chem. Soc. Perkin Trans. I*, 20 (2001) 2682-2689.
- [24] K. P. R. Kartha, R. A. Field, Iodine, and Its Interhalogen Compounds: Versatile Reagents in Carbohydrate Chemistry V. Synthesis of 1, 2-trans-Linked 1-Thioglycosides from the Per-O-acetylated Glycoses, *J. Carbohydr. Chem.* 17 (1998) 693-702.
- [25] R. J. Ferrier, R. H. Furneaux, Synthesis of 1, 2-trans-related 1-thioglycoside esters, *Carbohydr. Res.* 52 (1976) 63-68.
- [26] Y. M. Pu, B. Yagen, H. Ziffer, Stereoselective oxidations of a β -methylglycol, anhydrodihydroartemisinin, *Tetrahedron Lett.* 35 (1994) 2129-2132.
- [27] S. Oh, I. H. Jeong, W. S. Shin, S. Lee, Synthesis and antiangiogenic activity of exo-olefinated deoxyartemisinin derivatives, *Bioorg. Med. Chem. Lett.* 14 (2004) 3683-3686.
- [28] B. Venugopalan, P. Karnik, C. Bapat, D. Chatterjee, N. Iyer, D. Lepcha, Antimalarial activity of new ethers and thioethers of dihydroartemisinin, *Eur. J. Med. Chem.* 30 (1995) 697-706.
- [29] J.A Willoughby, S.N. Sundar, M. Cheung, A.S. Tin, J. Modiano, and G.L. Firestone, Artemisinin blocks prostate cancer growth and cell cycle progression by disrupting Sp1 interactions with the cyclin-dependent kinase-4 (CDK4) promoter and inhibiting CDK4 gene expression, *J. Biol. Chem.* 284 (2009) 2203-2213.
- [30] J. Hou, D. Wang, R. Zhang, H. Wang,. Experimental therapy of hepatoma with artemisinin and its derivatives: in vitro and in vivo activity, chemosensitization, and mechanisms of action. *Clin. Cancer Res.* 14 (2008) 5519-5530.

- [31] W. Gao, F. Xiao, X. Wang, T. Chen. Artemisinin induces A549 cell apoptosis dominantly via a reactive oxygen species-mediated amplification activation loop among caspase-9,-8 and-3. *Apoptosis* 18 (2013) 1201-1213.
- [32] Z. Wang, W. Hu, J. L. Zhang, X. H. Wu, H. J. Zhou, Dihydroartemisinin induces autophagy and inhibits the growth of iron-loaded human myeloid leukemia K562 cells via ROS toxicity, *FEBS Open Bio.* 2 (2012) 103-112.
- [33] H. Pelicano, D. Carney, P. Huang, ROS stress in cancer cells and therapeutic implications, *Drug Resist. Updat.* 7 (2004) 97-110.
- [34] B. Kumar, S. Koul, L. Khandrika, R. B. Meacham, H. K. Koul, Oxidative stress is inherent in prostate cancer cells and is required for aggressive phenotype, *Cancer Res.* 68 (2008) 1777-1785.
- [35] H. U. Simon, A. Haj-Yehia, F. Levi-Schaffer, Role of reactive oxygen species (ROS) in apoptosis induction, *Apoptosis* 5 (2000) 415-418.
- [36] J. M. Grad, X. R. Zeng, L. H. Boise, Regulation of Bcl-xL: a little bit of this and a little bit of STAT, *Curr. Opin. Oncol.* 12 (2000) 543-549.
- [37] I. Lebedeva, R. Rando, J. Ojwang, P. Cossum, C. A. Stein, Bcl-xL in prostate cancer cells: effects of overexpression and down-regulation on chemosensitivity, *Cancer Res.* 60 (2000) 6052-6060.
- [38] K. Nabeshima, T. Inoue, Y. Shima, T. Sameshima, Matrix metalloproteinases in tumor invasion: role for cell migration, *Pathol. Int.* 52 (2002) 255-264.
- [39] L. Zhang, J. Shi, J. Feng, H. Klocker, C. Lee, J. Zhang, Type IV collagenase (matrix metalloproteinase-2 and-9) in prostate cancer, *Prostate Cancer Prostatic Dis.* 7 (2004) 327-332.
- [40] J. DeGregori, G. Leone, A. Miron, L. Jakoi, J. R. Nevins, Distinct roles for E2F proteins in cell growth control and apoptosis, *Proc. Natl. Acad. Sci.* 94 (1997) 7245-7250.
- [41] E. J. Morris, J. Y. Ji, F. Yang, L. Di Stefano, A. Herr, N. S. Moon, E. J. Kwon, K. M. Haigis, A. M. Naar, N. J. Dyson, E2F1 represses β -catenin transcription and is antagonized by both pRB and CDK8, *Nature* 455 (2008) 552-556.

- [42] D. Greenbaum, C. Colangelo, K. Williams, M. Gerstein, Comparing protein abundance and mRNA expression levels on a genomic scale. *Genome Biol.* 4 (2003) 117.
- [43] A. Ryo, Y. C. Liou, G. Wulf, M. Nakamura, S. W. Lee, K. P. Lu, PIN1 is an E2F target gene essential for Neu/Ras-induced transformation of mammary epithelial cells, *Mol. Cell. Biol.* 22 (2002) 5281-5295.
- [44] J. P. Alao, The regulation of cyclin D1 degradation: roles in cancer development and the potential for therapeutic invention, *Mol. Cancer* 6 (2007) 2413-2419.
- [45] G. M. Wulf, A. Ryo, G. G. Wulf, S. W. Lee, T. Niu, V. Petkova, K. P. Lu, Pin1 is overexpressed in breast cancer and cooperates with Ras signaling in increasing the transcriptional activity of c-Jun towards cyclin D1, *EMBO J.* 20 (2001) 3459-3472.
- [46] H. Li, S. Wang, T. Zhu, J. Zhou, Q. Xu, Y. Lu, D. Ma, Pin1 contributes to cervical tumorigenesis by regulating cyclin D1 expression, *Oncol. Rep.* 16 (2006) 491-496.
- [47] Y. C. Liou, A. Ryo, H. K. Huang, P. J. Lu, R. Bronson, F. Fujimori, T. Uchida, T. Hunter, K. P. Lu, Loss of Pin1 function in the mouse causes phenotypes resembling cyclin D1-null phenotypes, *Proc. Natl. Acad. Sci.* 99 (2002) 1335-1340.
- [48] L. Bakiri, D. Lallemand, E. Bossy-Wetzl, M. Yaniv, Cell cycle-dependent variations in c-Jun and JunB phosphorylation: a role in the control of cyclin D1 expression, *EMBO J.* 19 (2000) 2056-2068.
- [49] R. Wisdom, R. S. Johnson, C. Moore, c-Jun regulates cell cycle progression and apoptosis by distinct mechanisms, *EMBO J.* 18 (1999) 188-197.
- [50] E. Shaulian, M. Karin, AP-1 as a regulator of cell life and death, *Nat. Cell Biol.* 4 (2002) E131-E136.
- [51] M. Kappelmann, A. Bosserhoff, S. Kuphal, AP-1/c-Jun transcription factors: regulation and function in malignant melanoma, *Eur. J. Cell Biol.* 93 (2014) 76-81.
- [52] W. Zhong, J. Peng, D. Wu, Z. Han, X. Bi, Q. Dai, Ki-67 and PCNA expression in prostate cancer and benign prostatic hyperplasia, *Clin. Invest. Med.* 31 (2008) 8-15.
- [53] J. J. Lu, L. H. Meng, U. T. Shankavaram, C. H. Zhu, L. J. Tong, G. Chen, L. P. Lin, J. N. Weinstein, J. Ding, Dihydroartemisinin accelerates c-MYC oncoprotein degradation and

- induces apoptosis in c-MYC-overexpressing tumor cells, *Biochem. Pharmacol.* 80 (2010) 22-30.
- [54] N. Xu, X. Zhou, S. Wang, L. L. Xu, H. S. Zhou, X. L. Liu, Artesunate Induces SKM-1 Cells Apoptosis by Inhibiting Hyperactive β -catenin Signaling Pathway, *Int. J. Med. Sci.* 12 (2015) 524-529.
- [55] C. M. Koh, C. J. Bieberich, C. V. Dang, W. G. Nelson, S. Yegnasubramanian, A. M. De Marzo, MYC and prostate cancer, *Genes & Cancer* 1 (2010) 617-628.
- [56] R.M. Jones, J. Branda, K.A. Johnston, M. Polymenis, M. Gadd, A. Rustgi, L. Callanan, E.V.Schmidt, An essential E box in the promoter of the gene encoding the mRNA cap-binding protein (eukaryotic initiation factor 4E) is a target for activation by c-myc, *Mol. Cell. Biol.* 16 (1996) 4754-4764.)
- [57] F.Meric, K.K.Hunt, Translation initiation in cancer: a novel target for therapy. *Mol. Cancer Ther* 1 (2002) 971-979.
- [58] H.G.Wendel, de Stanchina, E. Stanchina de, J.S.Fridman, A.Malina, S.Ray, S.Kogan, C.Cordon-Cardo, J.Pelletier, S.W.Lowe, Survival signalling by Akt and eIF4E in oncogenesis and cancer therapy, *Nature* 428 (2004) 332.
- [59] E.R.Hahm, K.B.Singh, S.V.Singh, c-Myc is a novel target of cell cycle arrest by honokiol in prostate cancer cells, *Cell Cycle* 15 (2016) 2309-2320.
- [60] T.Abbas, A.Dutta, 2009. p21 in cancer: intricate networks and multiple activities, *Nat Rev Cancer* 9 (2009) 400.
- [61] K. Lohr, C. Moritz, A. Contente M. Dobbstein, p21/CDKN1A mediates negative regulation of transcription by p53, *J. Biol.Chem.* 278 (2003) 36966-36972.
- [62] J. Yun, H. D. Chae, T. S. Choi, E. H. Kim, Y. J. Bang, J. Chung, K. S. Choi, R. Mantovani, D. Y. Shin, Cdk2-dependent phosphorylation of the NF-Y transcription factor and its involvement in the p53-p21 signaling pathway, *J. Biol. Chem.* 278 (2003) 36966-36972.
- [63] E. Warbrick, PCNA binding through a conserved motif, *Bioessays*, 20 (1998) 195-199.
- [64] H. Kim, M. Rafiuddin-Shah, H. C. Tu, J. R. Jeffers, G. P. Zambetti, J. J. D. Hsieh, E. H. Y. Cheng, Hierarchical regulation of mitochondrion-dependent apoptosis by BCL-2

subfamilies, *Nat. Cell Biol.* 8 (2006) 1348-1358.

- [65] S. N. Willis, L. Chen, G. Dewson, A. Wei, E. Naik, J. I. Fletcher, J. M. Adams, D. C. Huang, Proapoptotic Bak is sequestered by Mcl-1 and Bcl-xL, but not Bcl-2, until displaced by BH3-only proteins, *Genes Dev.* 19 (2005) 1294-1305.
- [66] Y. Meng, W. Tang, Y. Dai, X. Wu, M. Liu, Q. Ji, M. Ji, K. Pienta, T. Lawrence, L. Xu, L., Natural BH3 mimetic (-)-gossypol chemosensitizes human prostate cancer via Bcl-xL inhibition accompanied by increase of Puma and Noxa, *Mol. Cancer Ther.* 7 (2008) 2192-2202.

Highlights

- Novel *S*-linked dihydroartemisinin with potent anti-proliferative activity.
- Profound anti-cancer effect against prostate cancer cell line PC-3.
- Compound **9a** induced G1 cell cycle arrest and cell death.
- Inhibitory effect of **9a** on the expression of Pin1, cyclin D1, c-Myc & eIF4E.
- **9a** Reduced the migration potential of PC-3 cells and MMP-9 abundance.